

Camilla Mult Marnor

# Mapping distribution patterns of brittle stars using ROV-based imaging

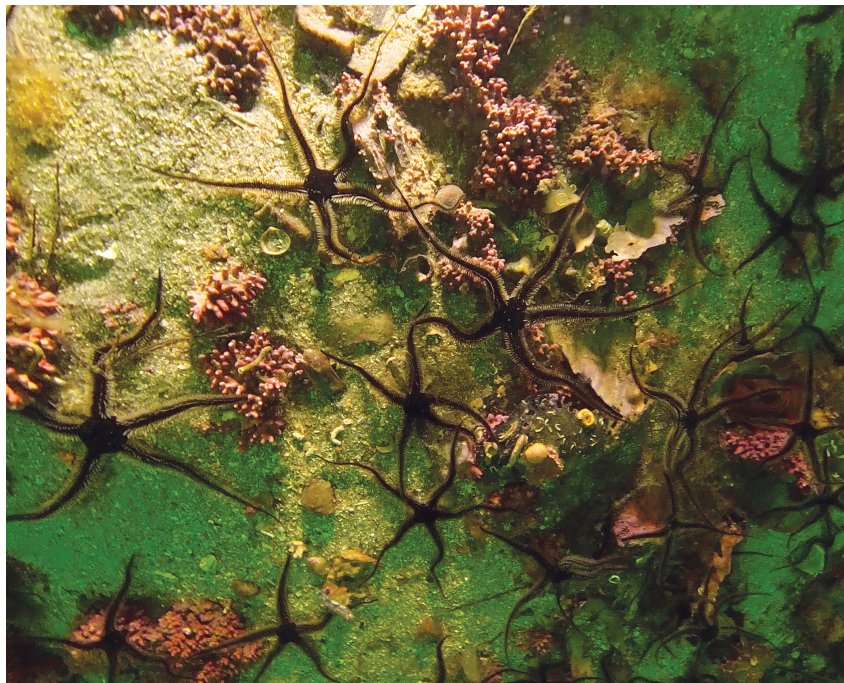
Master's thesis in Ocean Resources

Supervisor: Geir Johnsen

Co-supervisor: Torkild Bakken, Aksel Alstad Mogstad

May 2022

NTNU  
Norwegian University of Science and Technology  
Faculty of Natural Sciences  
Department of Biology





Camilla Mult Marnor

# **Mapping distribution patterns of brittle stars using ROV-based imaging**

Master's thesis in Ocean Resources

Supervisor: Geir Johnsen

Co-supervisor: Torkild Bakken, Aksel Alstad Mogstad

May 2022

Norwegian University of Science and Technology

Faculty of Natural Sciences

Department of Biology



Norwegian University of  
Science and Technology



## *Acknowledgements*

The work for this thesis took place at the Norwegian University of Science and Technology (NTNU), at the Department of Biology in the period from January 2021 to May 2022. The majority of the work was conducted at Trondheim Biological Station (TBS) and NTNU Sealab. Field work was performed at NTNU's field station at Sletvik. The project was funded by NTNU Centre for Autonomous Marine Operations and Systems (NTNU AMOS).

First, I want to thank my supervisor Geir Johnsen for his endless enthusiasm and encouragement, and for taking me out of my comfort zone by giving me a MSc project that was of an explorational nature. This has, in my opinion, increased my learning outcome and has inspired my curiosity and creativity. I would like to thank my co-supervisor Torkild Bakken for his guidance with taxonomic identification, assistance in the field and for valuable feedback and answers during the writing of the thesis. And my co-supervisor Aksel Alstad Mogstad for aid in concretizing the thesis, help with the statistics and for discussions of the results. In addition, I want to thank all three for inspiring me during my years at NTNU which has led me to where I am today.

A big thank you to Bjarne Kvæstad for taking the time and interest in my project to broaden its' and my perspective and teach me about machine learning (and then explain it over again several times during the past 6 months).

I want to thank Håvard Snefjella Løvås for teaching me how to use the ROV and for finding good solutions which pretty much defined the setup for the study.

I want to thank Rune Bjørgum for always being friendly, and for assisting me in the field, including rowing across Hopavågen and back so that I could explore some new areas. Thank you to Stephen Grant for answering my questions regarding the 360 camera. I also want to thank the people working at TBS for keeping the doors to their offices open and always being helpful, and for creating a good social environment.

To all my fellow students: thank you for making the time at NTNU memorable. And especially to my master group: Annecken Nøland, Malin Bø Nevstad, Maren Thu, Marte Søreng and Mikkel Bjerkvoll for assistance, support, discussions, and good memories from the past two years.

Last, but not least, I want to thank Kjetil Viste Levik, for his endless patience and support, for taking extra trips to Trondheim to support me during the final stages of the writing, and for even joining me on my last trip to Sletvik as my field assistant.

Trondheim, May 2022  
Camilla Mult Marnor

Front page: *Ophiocomina nigra* and red coralline algae. Photo: Camilla Mult Marnor



## ***Abstract***

A high demand for marine ecosystem services and competition for ocean space are pressing marine ecosystems to the limit. Efficient methods for identification, mapping and monitoring are needed to understand the dynamic processes of the marine environment and create a baseline for good management decisions. The aim of this study was to explore the potential of a 360 camera mounted to a small remotely operated vehicle (ROV) to identify, map and monitor the spatial distribution of brittle stars in shallow coastal areas. Transect lines were conducted to investigate three areas in three consecutive seasons. Images from the 360 camera were analyzed for the number of brittle stars, as well as variables related to the substrate and possible indicators of food availability. A multivariate statistical analysis was used to investigate connections between the different variables in the data set. Additionally, annotated images were used to train an algorithm for automatic identification of the species *Ophiocomina nigra* in images by machine learning.

*Ophiocomina nigra* was easily identified in images. A brittle star bed of this species was found on coarse sediment in one of the studied areas. The analysis indicated that the occurrence of other visible epifauna was low in this area. In the other areas *O. nigra* was observed to prefer hard elevated surfaces or patches of loose macroalgae. The patterns in spatial distribution can be connected to the flexibility in feeding methods exhibited by this species. Brittle stars in the genus *Ophiura* were not possible to identify to species level with this method. The spatial distribution of *Ophiura* sp. was correlated with fine sediments, which can be connected to their feeding on epifauna and infauna. The results showed that depth, season, and temperature was not determining factors for the distribution of brittle stars in this study.

Many factors influence the image quality and identification success of objects of interest (OOI), and trade-offs have to be considered in relation to the scope of the study. MiniROVs have the potential to allow for efficient data collection in marine environments, even by citizens. A 360 camera can substantially increase the information gained with little extra time use and expenses. Limitations was met in this study related to the lack of geopositioning and options for automatic speed and altitude of the miniROV. This is expected to be solved in newer models of the miniROV. The performance of the algorithm used for automatic identification of *O. nigra* with machine learning was an accuracy of 86.7% based on numbers identified by the algorithm compared to the numbers annotated manually. Automatic identification with machine learning can decrease time needed for image analysis substantially, which is necessary to transform large amounts of data into information that can be used for marine conservation and management.





## ***Sammendrag***

Stor etterspørsel etter marine økosystemtjenester og konkurranse om havrom presser marine økosystemer til det ytterste. Det er et behov for effektive metoder for identifisering, kartlegging og overvåking for å forstå dynamiske prosesser i det marine miljøet, og for å skaffe et informasjonsgrunnlag for gode forvaltningsavgjørelser. Målet med denne studien var å utforske potensialet til et 360-kamera montert på en liten fjernstyrt undervannsfarkost (ROV) for å identifisere, kartlegge og overvåke romlig utbredelse av slangestjerner i grunne kystområder. Transektlinjer ble utført for å undersøke tre områder over tre sesonger. Bilder fra 360-kameraet ble analysert for antall slangestjerner i tillegg til variabler knyttet til substrat og mulige indikatorer på mattilgang. En multivariat statistisk analyse ble brukt for å undersøke sammenhenger mellom de ulike variablene i datasettet. I tillegg ble annoterte bilder brukt til opptrening av en algoritme for automatisk identifisering av arten *Ophiocomina nigra* i bilder ved hjelp av maskinlæring.

*Ophiocomina nigra* var enkel å identifisere i bilder. En slangestjerneeng med denne arten ble oppdaget på grovt sediment i et av de studerte områdene. Analysen indikerte at det var lav forekomst av annen synlig epifauna i dette området. I de to andre studieområdene ble det observert at *O. nigra* foretrakk hardt og forhøyet substrat eller ansamlinger av løse biter av makroalger. Den romlige fordelingen av arten kan være knyttet til dens fleksibilitet til å benytte ulike fôringsstrategier. Slangestjerner i slekten *Ophiura* var ikke mulig å identifisere til art med metoden. Den romlige fordelingen av *Ophiura* sp. var korrelert med forekomst av fint sediment, noe som kan være knyttet til at disse artene spiser bunndyr i og på sedimentet. Resultatene viste at dybde, sesong og temperatur ikke var avgjørende faktorer for utbredelsen av slangestjerner i dette studiet.

Det er mange faktorer som påvirker bildekvaliteten og identifiseringssuksess av organismer av interesse (OOI) og ulike avveininger må gjøres ut ifra omfanget til studien som skal utføres. MiniROV'er har potensialet til å muliggjøre effektiv innsamling av data i marine miljøer, til og med av borgere. Et 360-kamera kan øke mengden innhentet informasjon betraktelig uten særlig økning i tidsforbruk og kostnader. Begrensninger med metoden ble oppdaget i denne studien knyttet til mangel på geoposisjonering og innstillinger for automatisk hastighet og høyde over havbunnen for miniROV'en. Det er forventet at disse utfordringene er løst i nyere modeller av miniROV'en. Algoritmen som ble brukt til automatisk identifisering av *O. nigra* med maskinlæring hadde en nøyaktighet på 86.7% basert på antall identifisert av algoritmen sammenlignet med antall som var annotert manuelt. Automatisk identifisering med maskinlæring kan redusere tidsbruk på bildeanalyser betraktelig, noe som vil være nødvendig for å kunne konvertere store mengder innsamlet data til informasjon som kan brukes til konservering og forvaltning.



## *Abbreviations*

<b>AI</b>	Automatic identification
<b>cDOM</b>	Colored dissolved organic matter
<b>Chl a</b>	Chlorophyll a
<b>CMOS</b>	Complementary metal-oxide-semiconductor
<b>EUNIS</b>	European nature information system
<b>FHD</b>	Full high definition
<b>FOV</b>	Field of view
<b>fps</b>	Frames per second
<b>HD</b>	High definition
<b>IOPs</b>	Inherent optical properties
<b>LED</b>	Light emitting diode
<b>Mbps</b>	Megabits per second
<b>MCA</b>	Multiple correspondence analysis
<b>MP</b>	Megapixels
<b>OOI</b>	Object(s) of interest
<b>RGB</b>	Red, green, blue
<b>ROV</b>	Remotely operated vehicle
<b>TSM</b>	Total suspended matter



## Table of contents

<i>Acknowledgements</i> .....	I
<i>Abstract</i> .....	III
<i>Sammendrag</i> .....	V
<i>Abbreviations</i> .....	VII
1 Introduction .....	1
1.1 Brittle stars - ophiuroids .....	1
1.1.2 <i>Ophiocomina nigra</i> .....	4
1.1.3 <i>Ophiura</i> sp. ....	5
1.2 Remotely operated vehicle (ROV) .....	6
1.3 Underwater photography .....	6
1.3.1 Digital photography .....	6
1.3.2 Resolution .....	7
1.3.3 Geometric distortion .....	7
1.3.4 Optical properties of seawater .....	8
1.4 Experimental aims .....	8
2 Materials and methods.....	10
2.1 Study area .....	10
2.2 Imaging techniques and platforms.....	12
2.2.1 MiniROV .....	12
2.2.2 360 camera.....	13
2.3 ROV transects.....	14
2.4 Processing of video material.....	14
2.4.1 Extracting transect videos from the 360 camera.....	14
2.4.2 Extracting video from the ROV.....	16
2.5 Image analysis .....	16
2.5.1 Identification of brittle stars .....	17
2.5.2 Other fauna .....	18
2.5.3 Substrate .....	19
2.6 Multiple correspondence analysis (MCA).....	20
2.7 Automatic identification of <i>Ophiocomina nigra</i> .....	23
3 Results .....	24
3.1 Habitat description.....	24

3.1.1	Location 1 .....	24
3.1.2	Location 2 .....	25
3.1.3	Location 3 .....	26
3.2	Multiple correspondence analysis (MCA).....	27
3.2.1	Contribution of variables .....	27
3.2.2	Distribution of samples within the different variables .....	29
3.2.3	The spatial distribution and density of <i>Ophiocomina nigra</i> related to the categorical variables .....	31
3.2.4	The numerical variables related to the dimensions of the multiple correspondence analysis (MCA) .....	32
3.3	Automatic identification with machine learning .....	33
4	Discussion.....	36
4.1	Assessing the spatial distribution of brittle stars .....	36
4.1.1	<i>Ophiocomina nigra</i> brittle star bed.....	36
4.1.2	<i>Ophiocomina nigra</i> on macroalgae and hard substrate .....	38
4.1.3	Spatial distribution of <i>Ophiura</i> sp. ....	38
4.1.4	The distribution of brittle stars in relation to temperature and depth .....	39
4.2	Factors influencing video and image quality.....	39
4.2.1	Field of view (FOV) .....	39
4.2.2	Settings for video resolution.....	40
4.2.3	The effect of a three-dimensional seascape .....	40
4.2.4	The effect of ambient light, water transparency and substrate .....	41
4.3	Study design with ROV transects.....	41
4.4	Future perspectives .....	42
4.4.1	Possibilities for the ROV with a 360 camera .....	42
4.4.2	<i>Ophiocomina nigra</i> as indicator .....	43
4.4.3	Machine learning and automatic identification (AI) .....	44
4.4.4	Citizen science .....	44
5	Conclusion .....	46
6	References .....	47

# 1 Introduction

The ocean is the largest ecosystem on the planet. The marine environment provides humanity with a range of ecosystem services, such as food, energy, carbon sequestration and coastal protection (Barbier, 2017; DNV, 2021). In turn, anthropogenic activity puts great pressure on marine ecosystems. Climate change, overfishing, habitat destruction and marine littering are only a few of the human-induced pressures that lead to loss of species and habitat diversity, which in turn reduces the resilience of marine ecosystems (Halpern *et al.*, 2008; DNV, 2021). There is a high demand for ocean space and this is predicted to keep accelerating (DNV, 2021). Information on the distribution of species and habitats and an understanding of the marine dynamic processes is essential to make informed management and conservation decisions (Palumbi and Hedgecock, 2005; Shumchenia and King, 2010; Buhl-Mortensen, Hodnesdal and Thorsnes, 2015).

The accessibility of benthic habitats has made them a challenge to study and understand. Traditionally, the understanding of the benthic environment has been based on destructive sampling techniques (e.g., cores, grabs, dredges). These methods do not give information on context, behavior, and interactions between the benthic species and between the benthic species and their habitat. Optical and acoustic sensors mounted on sensor carrying platform have provided non-destructive alternatives with a larger spatial extent and possibilities to investigate areas that previously were inaccessible (Solan *et al.*, 2003; Mogstad, 2021). Underwater imaging has provided a new understanding of benthic communities by giving a visual view over the environment and temporal variation in local processes (Parry *et al.*, 2003; Solan *et al.*, 2003).

The choice of sensor carrying platform and sensor must be adapted to the scope of the study (Mogstad, 2021). It is essential that the sensor can detect the target and that the scale is appropriate for the process under investigation (Davies *et al.*, 2001). Consequently, it is important to know the possibilities and the limitations of different methods. In addition, more efficient methods lead to large amounts of data, which needs to be processed, stored, analyzed, and visualized (Solan *et al.*, 2003).

## 1.1 Brittle stars - ophiuroids

Ophiuroidea is the largest class in the phylum Echinodermata with 2123 extant species (Stöhr, O'Hara and Thuy, 2022). The class has two orders: Euryalida (basket stars and snake stars) and Ophiurida (brittle stars) (Stöhr, O'Hara and Thuy, 2012; Hansson, Cedhagen and Strand, 2013). The information is limited on the global diversity of ophiuroids. Many species have been assigned to new taxonomic positions, and many species have not been reported since their initial description (Stöhr, O'Hara and Thuy, 2012). There is a large variation in lifestyles between species and they inhabit benthic habitats in all oceans, from shallow waters to great depths (Stöhr, O'Hara and Thuy, 2012). They play an important role in benthic-pelagic coupling, and

affect the distribution of benthic species due to high densities in some places (Piepenburg, 2000).

Ophiuroids deploy a range of feeding methods: deposit-feeding, suspension-feeding, scavenging and predation. Many species can alternate between different feeding methods (Warner, 1982; Stöhr, O'Hara and Thuy, 2012). Known predators of ophiuroids are crabs (e.g., *Necora puber* (Linnaeus, 1767)), fish (e.g., *Labrus bergylta* Ascanius, 1767, *Pleuronectes platessa* Linnaeus, 1758), and sea stars (e.g., *Asterias rubens* Linnaeus, 1758, *Marthasterias glacialis* (Linnaeus, 1758), *Luidia sarsii* Düben & Koren in Düben, 1844) (Aronson, 1989; Hughes, 1998; Guillou, Blanchet-Aurigny and Le Goaster, 2013).

The majority of species are unisexual, but some are hermaphrodites. Most species exhibit sexual monomorphism (Stöhr, O'Hara and Thuy, 2012). Reproduction is usually sexual with release of eggs and sperm into the water. Fertilized eggs develop into planktotrophic pluteus larvae. The larvae go through a metamorphosis and juvenile sink to the seafloor where they continue their life as benthos. Asexual reproduction is less common, by internal fertilization with brooding of eggs, larvae and juveniles in the gonads or bursae (gonadal chambers), or by fissiparity; division of the central disc and regeneration of both halves (Stöhr, O'Hara and Thuy, 2012; Hansson, Cedhagen and Strand, 2013).

#### **1.1.1.1 Anatomy**

Echinoderms are characterized by radial symmetry, usually with five rays, a calcium carbonate skeleton with plates or spicules, and tube feet connected to an internal water vascular system (ambulacra) (Southward and Campbell, 2006). Ophiuroids have a flat central disc with five (less commonly four or six and up to ten) slender arms that are clearly demarcated from the disc (Mortensen, 1924; Stöhr, O'Hara and Thuy, 2012). Arms are easily fragmented or shed during stress but are quickly regenerated. The mouth is located on the underside (ventral side) of the disc, closed by as many jaws with teeth or tooth papillae as there are arms (Stöhr, O'Hara and Thuy, 2012). The stomach is a simple sac. Intestine and anus are absent. The arms are flexible and are used for feeding, burrowing and movement, making ophiuroids the most mobile of the echinoderms. Tube feet (also called tentacles or podia) are located in two rows along the arms on the ventral side. Both arms and central disc are covered with plates that are central in identification. Two larger radial shields are found on the upper (dorsal) side of the central disc by the base of every arm. There are often several larger plates in the center of the disc, with one central plate in the middle, surrounded by five primary plates. There are four arm plates per joint: two lateral, one dorsal and one ventral. Every lateral arm plate has a row of arm spines on the outer edge (Figure 1) (Mortensen, 1924; Southward and Campbell, 2006).



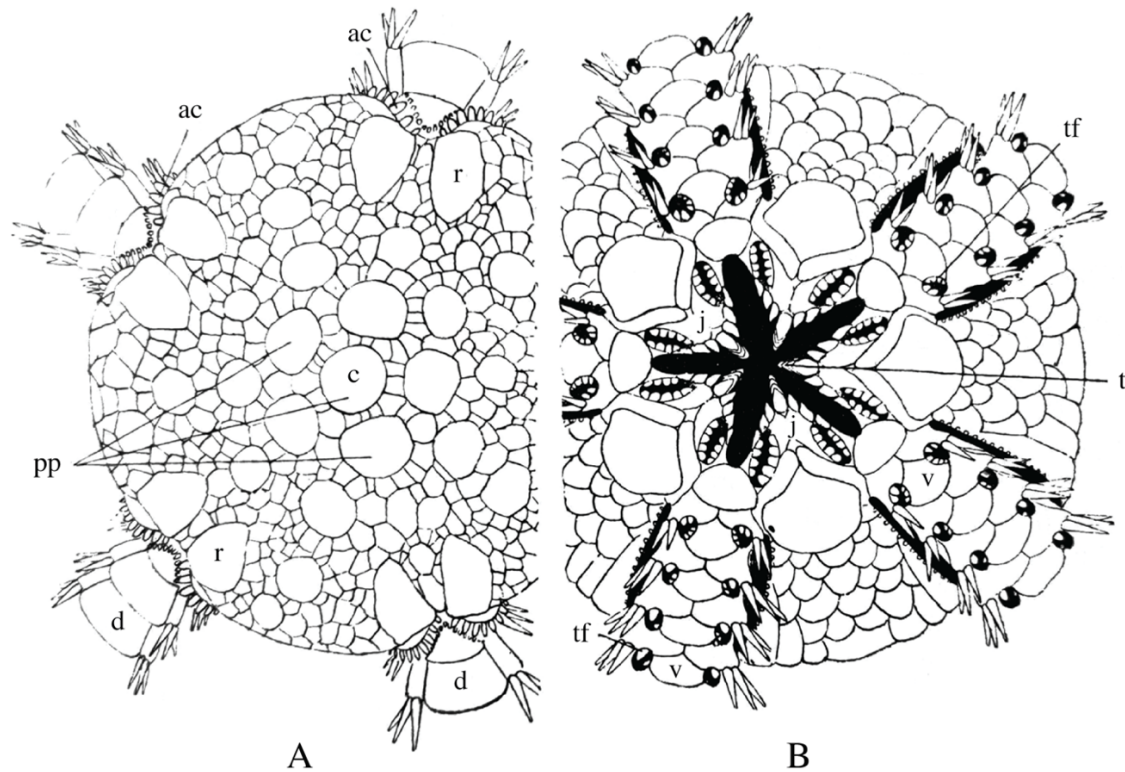


**Figure 1:** Central disc of an Ophiuroid. A – dorsal side, B – ventral side, ac – arm comb, c – central primary plate, d – dorsal arm plates, j – jaws, pp – primary plates, r – radial shield, t – teeth, tf – tube feet, v – ventral arm plates. Modified from Mortensen (1924).

### 1.1.1.2 Brittle star beds

Some species of brittle stars can often be found in large numbers, which can be a conspicuous component on the sea floor and be defining for the ecology of the habitat. In the European Nature Information System (EUNIS) for species and habitat types, there are several habitat types that include brittle stars. Brittle star beds of *Ophiothrix fragilis* (Abildgaard in O. F. Müller, 1789) and/or *Ophiocomina nigra* (Abildgaard in O. F. Müller, 1789) are described in habitat type A5.445 (European Environment Agency, 2019). Brittle star beds can cover large areas on the seafloor and contain millions of individuals. The two main bedforming species in this habitat type are *O. fragilis* and *O. nigra*. Brittle star beds of *Ophiopholis aculeata* (Linnaeus, 1767) occur on rare occasions. Species within the genus *Ophiura* Lamarck, 1840 can occur in large numbers on soft sediments, but usually not in densities comparable with the main bedforming species. Brittle star beds may be formed by one or a combination of the bedforming species. The phenomenon occurs on different types of substrates, ranging from hard to soft substrate. Gravel, cobbles and mixed coarse sediments are suggested to be the most frequent substrates (Hughes, 1998; De-Bastos and Hill, 2016). Several explanations have been proposed to explain the cause of brittle star aggregations; that it is connected to predation pressure (Aronson and Harms, 1985), primary production (Piepenburg, 2000), or organic enrichment (Blanchet-Aurigny *et al.*, 2012; Guillou, Blanchet-Aurigny and Le Goaster, 2013).

### 1.1.2 *Ophiocomina nigra*

*Ophiocomina nigra* is the only species in the *Ophiocomina* genus in Norway (Artsdatabanken, 2022). The species has a characteristic look with its dark brown to black color (Hansson, Cedhagen and Strand, 2013), sometimes with arm spines of a lighter color. The dorsal side of the central disc is covered in small granules, the radial shields are not visible and arm combs are absent (Mortensen, 1924). The disc diameter is up to 25 mm and arms up to 120 mm long. The species occurs down to 100 m depth on both hard substrate and coarse sand and gravel (Southward and Campbell, 2006; Hansson, Cedhagen and Strand, 2013). In Norway the species has been observed along most of the Norwegian coast, up to Harstad in the north (Artsdatabanken, 2022). The species is distributed to the Mediterranean and the Azores in the south. *Ophiocomina nigra* is usually found in sheltered to moderately exposed areas and can occur in high densities on the seafloor, sometimes mixed with *O. fragilis* (Hughes, 1998). It is a slow-growing and long-lived species which starts to reproduce at 3-4 years old and live up to 14 years (Hansson, Cedhagen and Strand, 2013).

#### 1.1.2.1 Feeding mechanisms

*Ophiocomina nigra* is an opportunistic feeder that can exploit a variety of food sources and it uses a range of feeding mechanisms (Fontaine, 1965; Moen and Svensen, 2020). Microphagous mechanisms comprise mucus net and surface film feeding. Macrophagous mechanisms are arm-loop capture, browsing and tube-foot capture.

**Mucus net feeding:** A type of suspension feeding. When exposed to a current, *O. nigra* will position itself into a “feeding position”: arms spread and extended upwards, curling at the tips, and the central disc slightly raised from the surface (Figure 2). The body is covered in a mucus secretion and mucus strands are extended between adjacent spines or spines and other parts of the body. One or several arms may be swept from side to side. *Ophiocomina nigra* will keep this position for a long time (6-8 hours, or longer) and use the mucus net to capture suspended particles (plankton, detritus) passing by with the current (Fontaine, 1965).

**Browsing:** *Ophiocomina nigra* has been observed to browse on laminarians and the fauna on them, and on carrion. It uses its teeth or oral tube feet to crush or tear food particles from the food source (Mortensen, 1924; Fontaine, 1965).

**Arm-loop capture:** A food particle is grasped by the tube feet (smaller particles), or the arm is flexed around the particle (larger particles) and brings it to the mouth.

**Tube-foot capture:** The tube feet transfer particles to the mouth. This method is used for particles too small for feeding by arm-loop capture.

**Surface film feeding:** A mechanism for grazing on detritus in the surface film of the water. Arms are moved parallel to the water surface. This method has mostly been observed in aquariums and is thought to be little used under natural conditions since the species lives in subtidal areas (Fontaine, 1965).

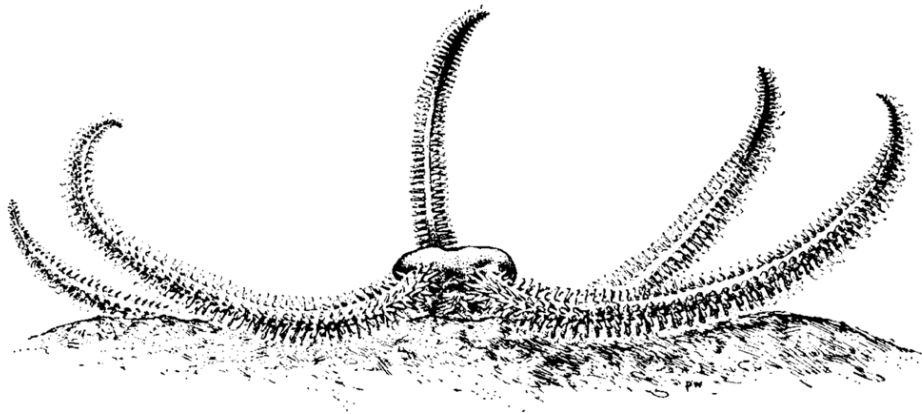


**Figure 2:** “Feeding position” of *Ophiocomina nigra* as described by Fontaine (1965) for mucus net feeding. When exposed to currents, *O. nigra* will take this position and its body will be covered in a mucus secretion, enhancing the capture of suspended particles in the water. Image from: Fontaine (1965).

### 1.1.2.2 Food

By examining gut contents, it has been found that *O. nigra* feeds on phytoplankton (diatoms, dinoflagellates), zooplankton (copepods, medusae), benthic invertebrates (small crustaceans, polychaetas, echinoderms), and sessile algae. Phytoplankton is an important food source year-round but due to spring blooms it is most important during this time of the year. Likewise, zooplankton is a dominating food source in late spring and early summer due to zooplankton blooms. During winter benthic invertebrates are a more important part of the diet. Sessile algae are considered to be a minor part of the food and restricted to those living in inshore areas (Taylor, 1958, as discussed by Fontaine, 1965). The species has also been observed to eat on carcasses of e.g. fish (Mortensen, 1924).

### 1.1.3 *Ophiura* sp.

Species of *Ophiura* have thin stiff arms that are short compared with other brittle stars. The arm spines are inconspicuous and are laying close to the arm in most species. The arms look like they are coming out from the dorsal side of the central disc, and arm combs are present (Mortensen, 1924; Southward and Campbell, 2006). There is no visible border between the dorsal and ventral side of the central disc (Hansson, Cedhagen and Strand, 2013). They have radial shields that often have a conspicuous color. It is easy to confuse different species within *Ophiura* (Moen and Svensen, 2020).

Species within *Ophiura* are predators on benthic prey (both epifauna and infauna), e.g., polychaetas, bivalves and crustaceans. They lay down on top of the prey or capture the prey by arm-loop (as described for *O. nigra* above). They also deposit feed on food particles associated with the sediment and scavenge carrion (Mortensen, 1924; Warner, 1982; Stöhr, O'Hara and Thuy, 2012). They are found on silt-covered rock surfaces or on substrates of gravel, sand or muddy sand (Hughes, 1998).

Five species from the genus are registered in Norway: *Ophiura carnea* Lütken, 1858, *Ophiura albida* Forbes, 1839, *Ophiura sarsii* Lütken, 1855, *Ophiura ophiura* (Linnaeus, 1758) and *Ophiura robusta* (Ayres, 1852). In Hopavågen two species are registered: *O. albida* and *O. ophiura* (Artsdatabanken, 2022). *Ophiura ophiura* is a large species with disc diameter up to 35 mm and arm length up to 120 mm. *Ophiura albida* is a smaller species with disc diameter up to 15 mm and arm length up to 60 mm (Southward and Campbell, 2006). Both species occur mainly on fine-grained sand and silt (Hansson, Cedhagen and Strand, 2013).

## 1.2 Remotely operated vehicle (ROV)

A Remotely operated vehicle (ROV) is an underwater platform that can carry optical and acoustic sensors and sampling devices (Ludvigsen, 2010). It is connected to the surface by an umbilical for two-way communication and power supply. ROVs have a range of applications related to scientific use, e.g., within biological, archeological, and geological studies. They make it possible to assess areas that are too deep for SCUBA diving, and vulnerable habitats (Ludvigsen, 2010). ROVs can provide valuable ground truthing for remotely sensed data from surface and aerial vehicles and satellites (Johnsen *et al.*, 2013; Mogstad, 2021), and a context to point samples (Ludvigsen, 2010). The umbilical connection to the surface gives power supply to orientation and environmental sensors, which extend the possible work time, and enables live video and control (Johnsen *et al.*, 2013). Disadvantages with ROVs are that they rely on power and communication through the umbilical, which limit the spatial range. They are also dependent on an operational vessel and specialists which leads to high operational costs (Johnsen *et al.*, 2013; Mogstad, 2021).

MiniROVs are small ROVs that are mainly intended for observational purposes. They are usually equipped with a camera, with limited options for adding additional sensors. As they are more transportable and can be deployed and recovered from shore or a small boat (Mitchell and Coggan, 2007), they offer a cost- and time efficient option for applications as video-based inspections of underwater structures and habitats (Mogstad, 2021). They can access shallower areas than the larger ROVs but are limited by size and power (Strømsholm, 2018).

## 1.3 Underwater photography

### 1.3.1 Digital photography

Digital cameras have a photosensor (hereafter: sensor) that records the light that enters the camera through the lens. The sensor transforms the light into an electrical signal (i.e., photons into photoelectrons). The processor converts this signal into a digital value which is stored in the memory card. A larger sensor can collect more light. The sensor has many pixels (also called photosensors, photosites, or photodiodes) which each convert light to a signal. For RGB (red, green, blue) cameras each pixel has a filter that allows it to register light from either the red, green, or blue part of the electromagnetic spectrum. The accurate RGB color for each pixel is then interpolated by algorithms in the camera. Each pixel on the sensor is connected to a pixel in the resulting image (Gietler, 2018). A high number of pixels on a sensor gives a high level

of detail. Fewer, but larger pixels on the same sized sensor can detect more light per pixel and increase the sensitivity of the sensor at the expense of spatial resolution.

### **1.3.2 Resolution**

Four categories of resolution are relevant for optical sensors regarding their ability to detect a specific process or an object of interest (OOI). These are spatial, spectral, radiometric and temporal resolution (Johnsen *et al.*, 2013). The spatial resolution of a sensor is the size of the smallest feature that can be detected with the sensor. This is the size of the area on the ground represented by one pixel for digital images (Davies *et al.*, 2001). The spatial resolution is affected by the distance between the sensor and the OOI and the signal-to-noise ratio of the sensor (Johnsen *et al.*, 2013). Spectral resolution is the ability of a sensor to distinguish between different intervals of wavelengths (Canada Centre for Mapping and Earth Observation, 2019). For instance, a RGB sensor is sensitive to wavelengths in the red (650 nm), green (550 nm) and blue (450 nm) parts of the electromagnetic spectrum (Johnsen *et al.*, 2013; Canada Centre for Mapping and Earth Observation, 2019). Radiometric resolution is the ability of the sensor to detect different light intensities (i.e., the dynamic range of the sensor). A high radiometric resolution enhances the sensor's ability to depict a range from very bright to dark areas. Temporal resolution is the revisit-time. This is a highly relevant concept for studying and understanding biological processes. To be able to assess changes between visits, geocalization of high accuracy is important (Johnsen *et al.*, 2013).

### **1.3.3 Geometric distortion**

An image is representing the Earth's three-dimensional surface in two dimensions and will have geometric distortions. The distortion is dependent on several factors, e.g., the altitude, attitude and velocity of the sensor carrying platform, the terrain, the curvature of the earth, and the perspective of the sensor (Canada Centre for Mapping and Earth Observation, 2019). Fisheye and wide-angle camera lenses give geometrically distorted images due to a larger image field of view (FOV) than the camera sensor. This leads to barrel distortion, where image points away from the center are displaced outwards from the ideal position (Park, Byun and Lee, 2009). When an optical sensor is photographing an OOI vertically from above (zenith view), objects to the side of the nadir (directly under the sensor) will appear to be leaning away from the nadir, and the top and side of the objects will be visible in the image (Figure 3) (Canada Centre for Mapping and Earth Observation, 2019).

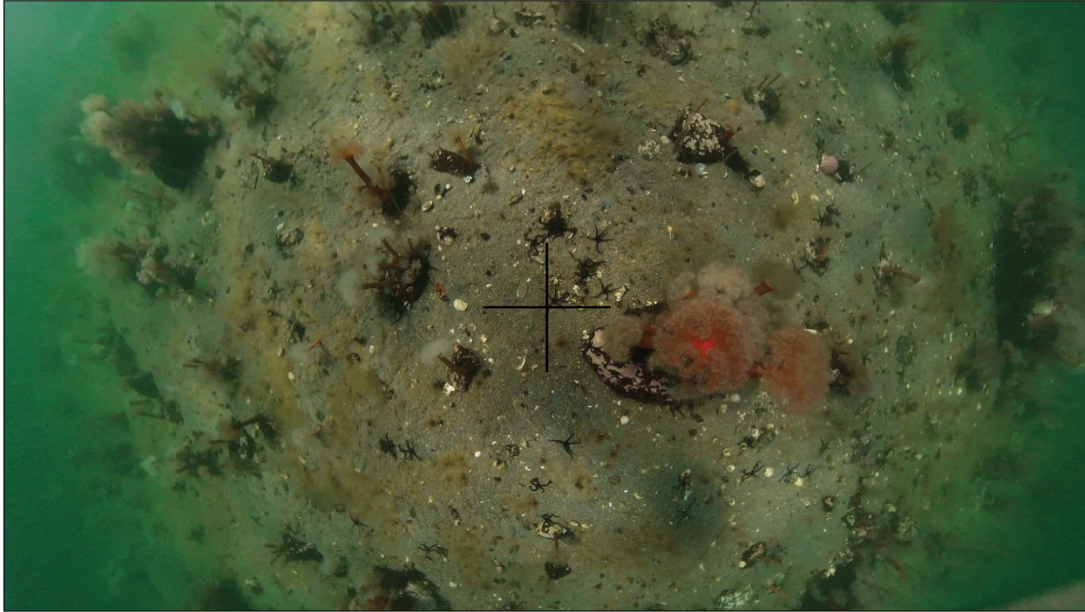


**Figure 3:** Example of geometric distortion from a fisheye camera lens. Objects directly under the sensor (i.e., at the nadir) are viewed from above. Objects to the side of the nadir are imaged both from above and the side. Photo: Camilla Mult Marnor.

### 1.3.4 Optical properties of seawater

Light behaves differently in water than in air, and this is important to account for when working with optical methods in marine environments (Funk, Bryant and Heckman Jr, 1972; Johnsen *et al.*, 2020). The quantity and spectral quality of light decreases rapidly as it moves through the water column due to absorption and scattering of photons. How far the light can penetrate depends on suspended particles in the water. Light penetrates shorter in coastal waters than in the open sea, usually up to 50 m depth (Kaiser *et al.*, 2011). Light attenuation is the sum of absorption and scattering. Light is attenuated in seawater due to the inherent optical properties (IOPs) of the seawater: the water itself absorbs and scatters light, phytoplankton absorbs and scatters light, colored dissolved organic matter (cDOM) absorbs light, and total suspended matter (TSM) scatters light. Water where attenuation is mainly caused by phytoplankton and the water itself gets a green to blue hue in images because seawater attenuate red light and phytoplankton (Chl a) has absorption peaks in blue and red wavelengths. cDOM absorbs light with blue to green wavelengths and water dominated by cDOM will get a yellow hue. TSM comprise particles suspended in the water that scatter light and affects the contrast and sharpness in images (Ludvigsen, 2010; Kjerstad, 2014).

## 1.4 Experimental aims

The aim of this study was to explore the potential of a 360 camera mounted on a miniROV to identify, map and monitor the spatial distribution of brittle stars in shallow coastal areas. The miniROV was used to drive transect lines that were visited in three consecutive seasons. Images from the 360 camera were analyzed for the number and species of brittle stars, as well as other

biotic and abiotic variables. A multivariate statistical analysis was performed to identify correlations between the registered variables. In addition, automatic identification of one brittle star species by machine learning was tested. The results of the study were used to discuss (1) whether the observed brittle star species expressed distribution patterns that could be connected to the abiotic and biotic variables that were registered; (2) factors influencing the quality of data obtained with the method; (3) the potential of automatic identification by machine learning for efficient image analysis; and (4) the potential of the method for mapping and monitoring benthic habitats in the future.

## 2 Materials and methods

### 2.1 Study area

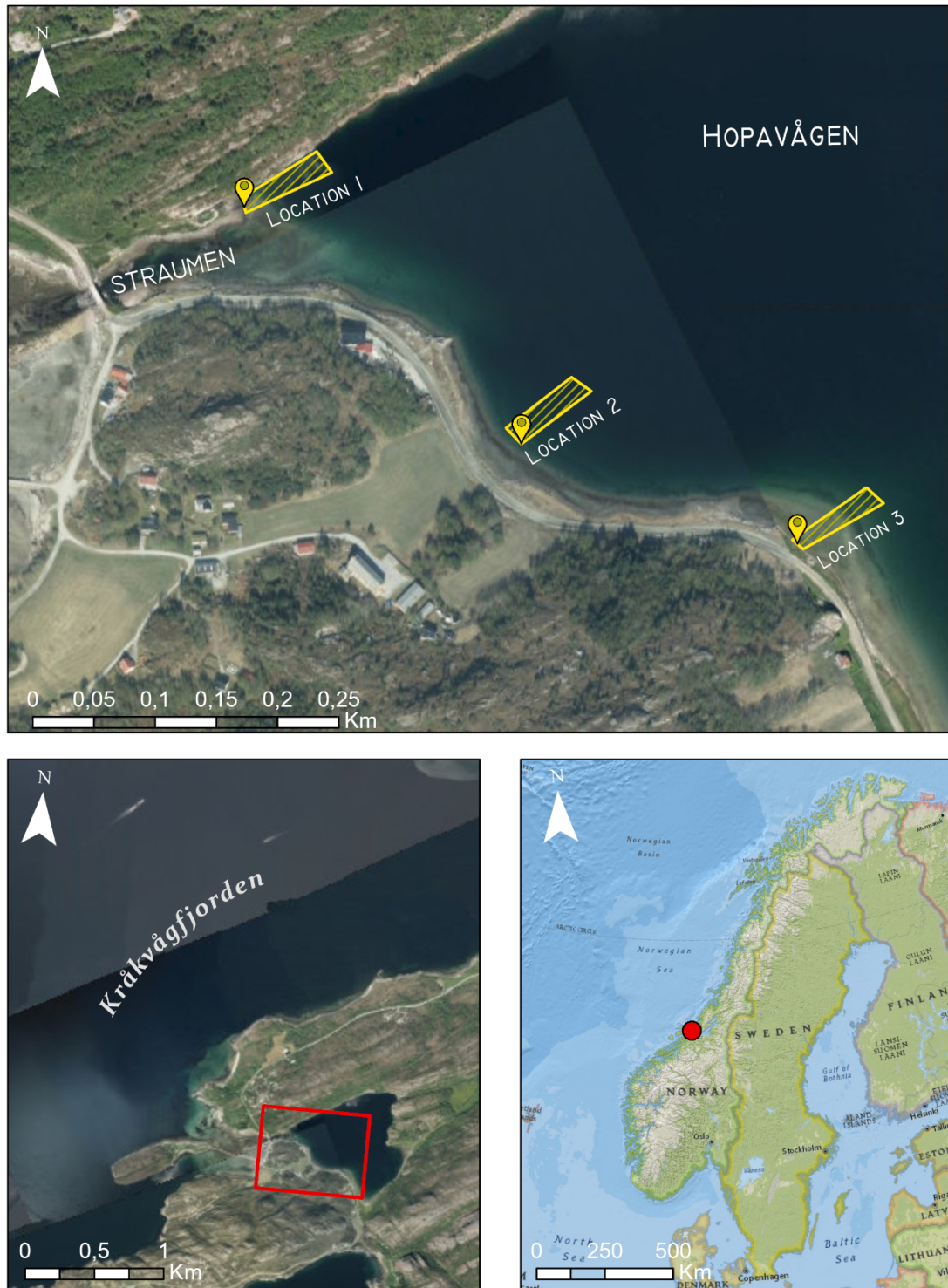
The study was conducted in Hopavågen, Agdenes, Trøndelag (63°35'37.8"N 9°32'44.5"E) in May, September, and November 2021.

Hopavågen is a small bay connected to Kråkvågfjorden by a narrow and shallow channel in the west (hereafter called “Straumen”). The area of Hopavågen is 370 000 m<sup>2</sup>, maximum depth is 31 m and average depth 18 m. The shallow sill leads to delayed tidal movements and a smaller tidal range inside the bay compared to the fjord. There is a variation between neap and spring tides in the delay and the time between high/low tide. Marion (1996) observed a tidal range of 0.32-0.70 m which corresponds to an exchange of water per tidal cycle of 118 400-259 000 m<sup>3</sup> out of the total volume of 6 660 000 m<sup>3</sup>. The reduced renewal of the water in the bay has led to stagnant deep water and a dead zone in the deepest areas with oxygen depletion and hydrogen sulfide. There are some small freshwater runoffs into Hopavågen, but the amount of freshwater is considered to be insignificant compared to the volumes of seawater that enters through Straumen every day (Marion, 1996).

Transect lines were conducted from land and out in three different locations (Figure 4). Each location was surveyed during visits to Hopavågen in three consecutive seasons: in May, September, and November 2021. Weather conditions for each sampling period is given in Table 1. The three locations chosen for transects were:






- **Location 1** (63°35'38.3"N 9°32'11.7"E): one area close to Straumen, following the rock wall on the north-west side of Hopavågen. This area was expected to be the most exposed to currents due to its closeness to Straumen. Max depth 7.8 m.
- **Location 2** (63°35'32"N 9°32'28"E): following a pipeline on the south side of the bay. Max depth 8.2 m.
- **Location 3** (63°35'29.3"N 9°32'44.3"E): a shallow area further east. Max depth 2.7 m.





**Figure 4:** Hopavågen ( $63^{\circ}35'37.8''\text{N}$   $9^{\circ}32'44.5''\text{E}$ ) with transect locations. The bottom maps show the study area marked in red. The top map shows the locations of the three transect lines that was performed by a Remotely Operated Vehicle (ROV) during surveys in May, September, and November 2021. Basemaps from the Norwegian Mapping Authority 2021 and ESRI National Geographic World Map 2021. Datum: WGS 1984, Projection: UTM Zone 32 N.

**Table 1:** Weather conditions and tidal data for the different fieldwork dates in Hopavågen. Temperature and wind are the average for the time period and max gust the highest measured gust. The weather data is measured at the closest weather station, Ørland metrological station, 12.9 km from Hopavågen (www.yr.no). Tidal data is from Kartverket.no for “Slettvika”. Note that there is a delay and a lower tidal range inside Hopavågen compared to Slettvika.

Date	Time	Areas visited	Weather	Temperature (°C)	Wind (max gust) (m/s)	Tide (cm)	Comments
05.05.21	11:30-15:00	Location 2 Location 3		9.2	9.4 (12.9)	128-82 (sinking, low tide, rising)	Low tide 14:19, 76 cm
06.05.21	15:35-16:05	Location 1		8.7	5.0 (8.5)	71-74 (low tide - rising)	Calm conditions, sun
06.09.21	15:15-16:45	Location 1		12.5	2.7 (5.2)	157-89 (sinking)	
09.09.21	10:15-11:10	Location 2 Location 3		12.2	7.1 (9.9)	91-174 (rising)	Heavy rainfall the days before. cDOM, freshwater runoffs
29.11.21	11:00-13:30	Location 1 Location 2 Location 3		-3.8	9.2 (12.4)	148-125 (sinking – low tide)	Wind, clouds

## 2.2 Imaging techniques and platforms

### 2.2.1 MiniROV

The miniROV used for this study was the Blueye Pioneer (Blueye Robotics, Norway), named ROV hereafter (Figure 5). Of orientation sensors, the ROV has an accelerometer, gyroscope, magnetometer, and sensors for depth and internal pressure. Environmental sensors include sensors for drone and water temperature, and a high definition (HD) camera in the front of the ROV (see Table 2 for camera specifications). A light emitting diode (LED) light (3300 lumen) is positioned under the camera (Blueye.no, 2022). The pressure sensor giving information on depth is located in the upper part of the drone (M. Ludvigsen, personal communication, November 2021). Thus, the depth stated corresponds to the distance between the top of the drone and the surface. The ROV is equipped with 4 thrusters: 2 in rear section, 1 vertical in the center and 1 lateral. It has a maximum speed of  $1.5 \text{ ms}^{-1}$  and can handle currents up to  $1 \text{ ms}^{-1}$ . The run-time is 2 hours for normal operations (not defined by producer), and extra batteries can be brought to extend the run-time.

The ROV is connected to a surface Wi-Fi router with a copper tether for two-way communication and power. For this study a 75 m long tether was used. The Wi-Fi router enables wireless communication with smartphones and tablets. The ROV is controlled with the Blueye app for Android/iOS phones or tablets, and it can be connected to a gaming controller. The display shows live video from the drone, heading, depth of the ROV, temperature, and battery status for the ROV, surface unit and mobile phone (Figure 5). Controller options include auto-heading and auto-depth (horizontal and vertical locking respectively), options to start/stop video recording, take a frame grab, and turn on/off the LED light.

### 2.2.2 360 camera

The 360 camera that was used was Insta360 One X2 (Arashi Vision, China) (except for in Location 1 in May, where the previous model Insta360 One X1 was used). This camera has two ultra-wide fisheye lenses with 200 degrees field of view (FOV), and the video and images are automatically stitched together to give a 360 view in the software Insta360 Studio 2021 (version 4.0.1, Arashi Vision, China). Camera sensor specifications are listed in Table 2. The camera was set to capture images at 30 frames per second (fps) at a spatial resolution of 5.7 K (about 5700 pixels horizontally on the photosensor). The 360 camera has a 6-axis gyroscope for orientation and stabilization. It is waterproof down to 10 m depth, and to 45 m with a dive case (Insta360.com, 2022). For this study a dive case was used, and the 360 camera was put on a GorillaPod (Joby GorillaPod 3K) with one leg removed and attached to the front of the ROV (Figure 5). The 360 camera was started and stopped manually.

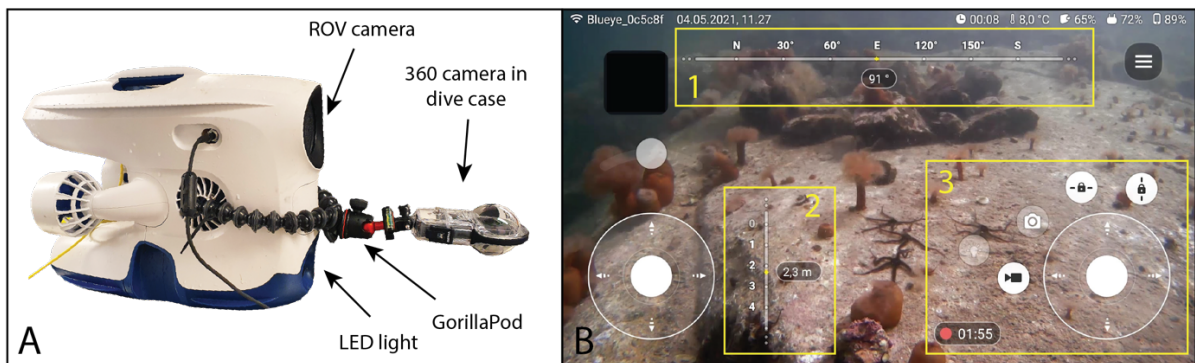


**Figure 5:** (A) Setup of the ROV for the study. The ROV had an integrated camera and a LED light. A 360 camera in a dive case was attached to the ROV with a GorillaPod. (B) The display in the Blueye app: (1) Heading of ROV in degrees, (2) depth of ROV in meters, (3) control options for video, frame grab, LED light, auto heading and auto depth. Photo: Camilla Mult Marnor.

**Table 2:** Camera sensor specifications for the camera of the ROV (Blueye Pioneer) and the 360 camera (Insta360 One X2).

	<b>Blueye Pioneer</b>	<b>Insta360 One X2</b>
<b>Video resolution</b>	FHD:1920x1080, 25/30 fps HD: 1280x720, 25/30 fps	5.7K: 5760x2880, 30 fps 4K: 3840x1920, 50 fps 3K: 3008x1504, 100 fps
<b>Sensor</b>	CMOS	CMOS
<b>Sensor size</b>	1/3 inch (4.8x3.6 mm)	1/2.3 inch (6.17x4.55 mm)
<b>35 mm equivalent focal length</b>	-	7.2 mm
<b>Aperture</b>	-	F2.0
<b>Video bitrate</b>	2 to 16 Mbps	100 Mbps
<b>Video format</b>	MP4	INSV

## 2.3 ROV transects

Areas of interest were chosen based on previous observations from SCUBA diving and field work in the area (Alvsvåg, 2017; Teacă, Ungureanu and Mureşan, 2017; G. Johnsen & H. Løvås, personal communication, May 2021), and a pre-survey by the use of a paddle board and GoPro 7 (Woodman Labs, USA) mounted on a camera stick. The initial geo-position on land for the three locations was registered using Google Earth. The ROV was placed in the desired direction and the heading (Figure 5 B.1) used as reference to drive the ROV in a straight transect. The ROV was driven from the shore and out to the extent of the tether (75 m). The ROV LED light was not used during transects, only natural light.

## 2.4 Processing of video material

Video from the ROV and the 360 camera was compared to find where the videos were matching to get video from the same segment from both cameras, and to be able to combine data from the ROV with imagery from the 360 camera. Frame grabs were then extracted from both sets of videos.

### 2.4.1 Extracting transect videos from the 360 camera

The 360 video was viewed and edited in the software Insta360 Studio 2021. The orientation and FOV of the edited video are set by making key frames. In a key frame the orientation and FOV for that exact moment in the edited video is decided by moving around in the image or setting desired values for the different options of the key frame (Figure 6). Identical key frames were added to the beginning and end of the videos, giving a constant orientation and FOV throughout the video.

The orientation was chosen so that the ROV was in the direction of the bottom of the image and the direction of movement at the top of the image. In addition to the identical key frames at the start and end of the video, “direction lock” was used to keep the orientation throughout the whole video. However, this did not work for all videos (Location 3 September and Location

2 May). The video from Location 2 May was constantly rotating throughout the whole video and this might have been an error with the gyroscope of the 360 camera. For Location 3 September the video was rotated 180 degrees and the direction of movement was towards the bottom of the image. This was possible to correct for later by rotating the images 180 degrees. The values for FOV control and Distortion angle (Figure 6) were kept the same for all videos, while the other values had to be adapted to the individual video. The aim was to get images that were showing the seafloor directly from above (zenith view), with as large FOV as possible without getting too much distortion at the edges of the images. See comparison of FOV in Figure 7.

The edited video was exported as a mp4 file with spatial resolution 1920x1080 image pixels. Next, the video was imported to SnapMotion (Vizzini, 2020), a software that generates frame grabs. The interval was set to every 5 seconds, including the start frame but not the end frame.

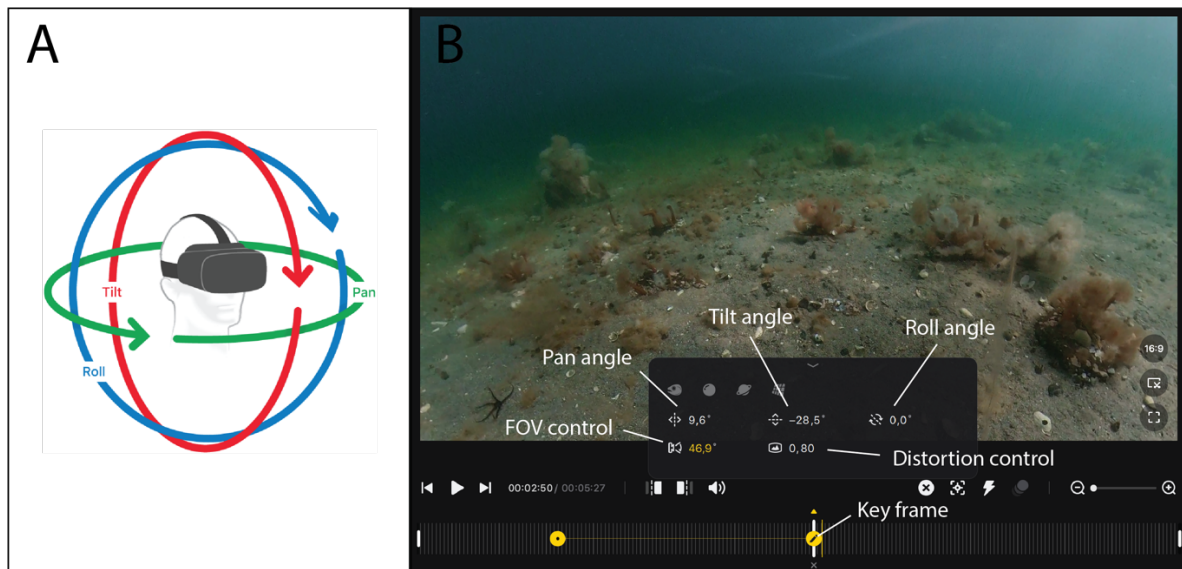


**Figure 6:** (A) The orientation of the field of view (FOV) of a 360 video can be changed by adjusting the pan (horizontal adjustment of FOV), tilt (up/down adjustment of FOV), and roll (sidewise rotation). (B) Insta360 Studio, software for viewing and editing 360 videos. FOV for edited video is set by making key frames. FOV is set for each key frame by adjusting values for pan angle, tilt angle, roll angle, FOV control and distortion control. FOV control adjusts the size of FOV (zooms in/out). Distortion control is related to the geometric distortion that results from a fisheye lens (straightens the horizon or increases its curvature), and this option also affects the size of FOV. Photo: Apple.com (A), Camilla Mult Marnor (B).

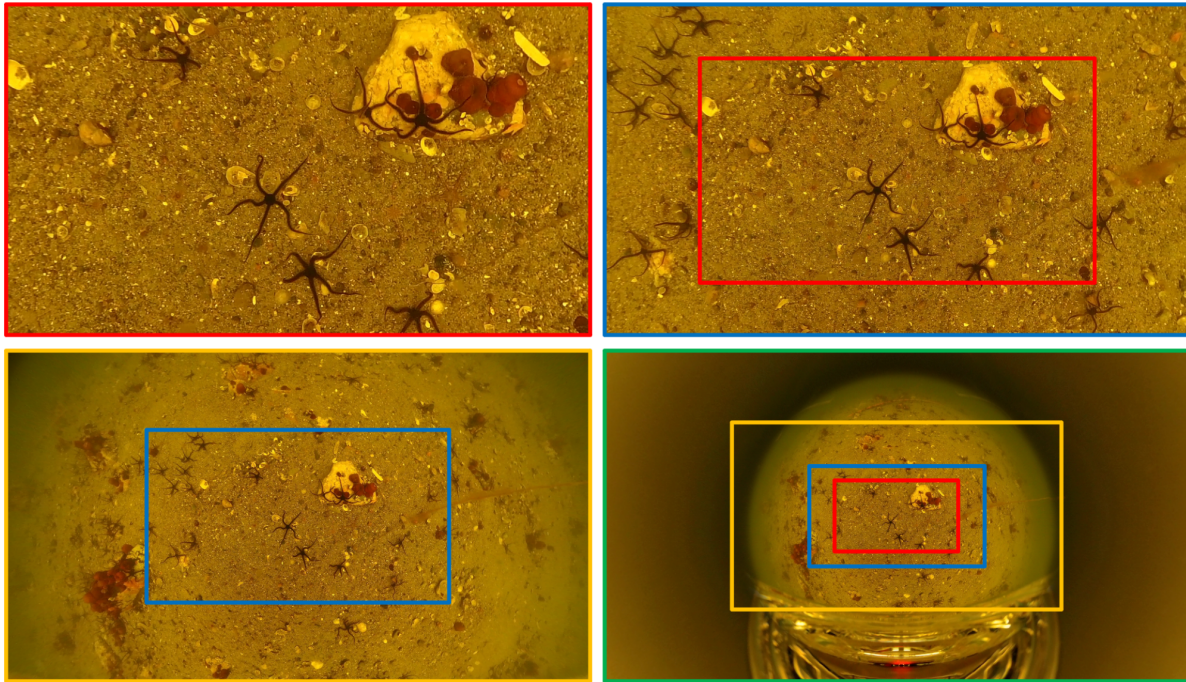


**Figure 7:** Comparison of different fields of view (FOV) from the 360 camera, from maximum magnification (FOV covers a small area) (red) to a wide angle FOV (green). The blue frame is what was used for the image analysis. Photo: Camilla Mult Marnor.

## 2.4.2 Extracting video from the ROV

The videos from the ROV from May had the dive information (depth, temperature, heading) as a separate subtitle file. The HandBrake software (HandBrake Team, 2022) was used to get the subtitle permanently overlaid on the video file. Between May and September there was an update on the ROV so that the dive information was automatically in the video from September and onwards. The videos were edited in QuickTime Player (Apple, USA) to fit the 360 video according to section 2.4. Frame grabs were extracted from the videos with SnapMotion in the same way as for the 360 videos. However, the dive information would disappear from the frame grabs from May when SnapMotion was used, so frame grabs from this month had to be extracted manually and named with the correct timestamp.

## 2.5 Image analysis

A total of 383 images from each camera were imported to Microsoft PowerPoint (Microsoft, USA), with corresponding images from the 360 camera and the ROV next to each other on a slide. This was to get an overview over the different views from the two cameras, and the dive information (temperature, depth, heading) from the ROV. The images from the 360 camera were analyzed for the number of brittle stars (to lowest possible taxonomic level), substrate type, and other fauna. Brittle stars were annotated with a colored dot according to their taxonomic identification. A subjective evaluation of the density of *O. nigra* was also registered for each image. 27 images were too blurry or too far away to see and/or count brittle stars and register substrate type, and were removed, giving a data set consisting of 356 images.

## 2.5.1 Identification of brittle stars

### 2.5.1.1 *Ophiocomina nigra*

Identification of *O. nigra* was done based on their characteristic dark color. Individuals of *O. nigra* were registered where the central disc was visible, or when black arms in a star shape were visible (in areas/images where *O. nigra* was already present), or where arms raised in the characteristic feeding position of the species were visible (Figure 2).

### 2.5.1.2 *Ophiura* sp.

As it is not possible to investigate mouth parts or dorsal plates on the central disc close enough for identification to species level of *Ophiura* (Southward and Campbell, 2006; Hansson, Cedhagen and Strand, 2013), these individuals were only identified to genus level. They were identified based on their characteristic shape with straight stiff arms with inconspicuous arm spines, and reddish brown to grey colors (Southward and Campbell, 2006).

*Ophiecten affinis* (Lütken, 1858) is a species that looks similar to the *Ophiura* species and is a common species along the Norwegian coast (Hansson, Cedhagen and Strand, 2013; Artsdatabanken, 2022). With a disc diameter up to 8 mm and arm length up to 25 mm it is smaller than the *Ophiura* species that have previously been registered in Hopavågen. As smaller individuals of what was thought to be *Ophiura* sp. was registered, it is possible that some of these could have been *O. affinis*. However, this is assumed not to be of importance for the aims of this study as this species has a similar life style as *Ophiura* sp. (Ambrose, 1993).

### 2.5.1.3 Density of *Ophiocomina nigra*

Due to the lack of a size reference and information of aerial coverage of the images, it was not possible to quantitatively describe the density of *O. nigra*. Instead, the images were assigned a qualitative *O. nigra* density category based on a subjective understanding of the appearance and image coverage (Figure 8):

- **Absent:** No *O. nigra* present in the image.
- **Low:** A few individuals present.
- **Medium:** *O. nigra* covers a large part of the image, or many individuals are densely aggregated in some areas.
- **High:** *O. nigra* covers most of the image.

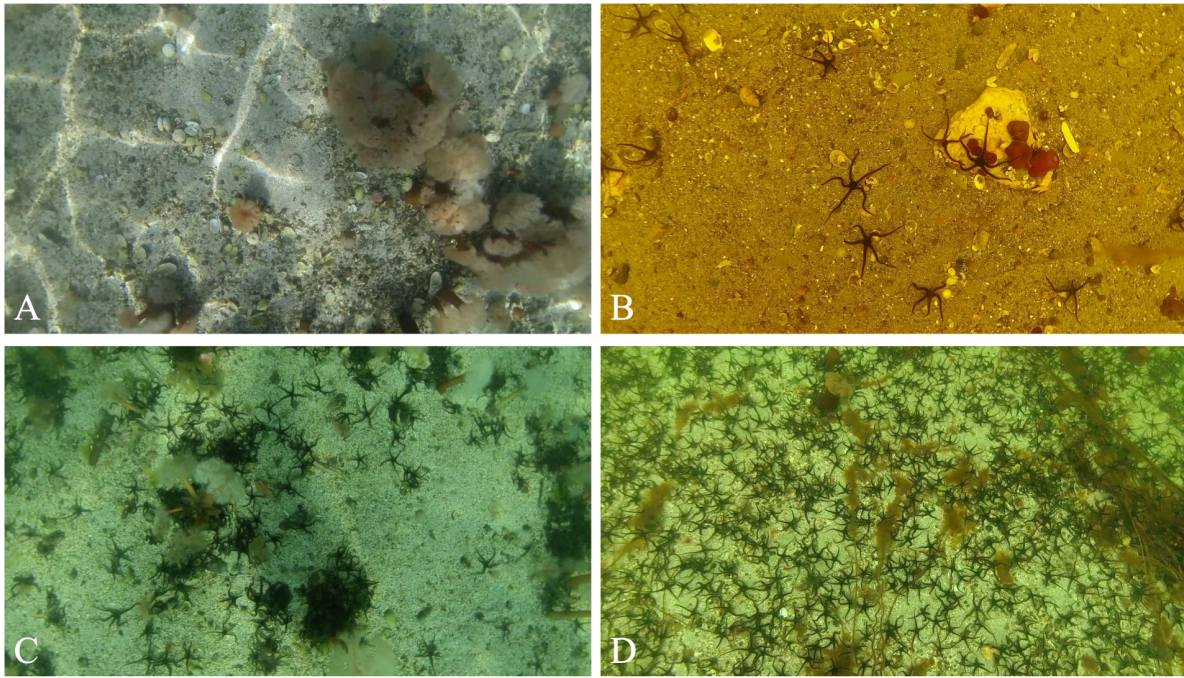


**Figure 8:** Examples of the different qualitative density categories for *Ophiocomina nigra* used in the image analysis: (A) Absent, (B) Low, (C) Medium, (D) High. Photo: Camilla Mult Marnor.

### 2.5.2 Other fauna

Non-ophiuroid organisms observed in the images were categorized into functional groups based on feeding strategies according to Table 3. The functional groups were based on those used by Iken *et al.* (2001). Many organisms use several feeding strategies but were categorized according to what was considered to be the main feeding strategy (De Ridder and Lawrence, 1982; Jangoux, 1982; Riisgård and Banta, 1998; Teacă, Ungureanu and Mureşan, 2017; Capa, 2021). The functional groups were:

- **Suspension feeders (Susp):** Feed on food particles suspended in the water column.
- **Deposit feeders (Dep):** Feed on food particles associated with the sediments.
- **Predators/scavengers (PredScav):** Move actively/hunt to capture prey, or feed on dead biomass.

For the image analysis, the presence of organisms from one or several of the functional groups was recorded as categories containing all occurring combinations of the three groups (Table 4).



**Table 3:** Other fauna that were registered in the images and their categorization into functional groups based on feeding strategies: Suspension feeders (Susp), deposit feeders (Dep), predators/scavengers (PredScav).

Phylum	Group	Presumptive Taxon	Functional group
Cnidaria	Actiniaria (order)		Susp
	Spirularia (order)	Cerianthidae Milne Edwards & Haime, 1851	Susp
Mollusca	Bivalvia (class)		Susp
	Gastropoda (class)		PredScav
		<i>Littorina</i> sp. Férussac, 1822	PredScav
Echinodermata	Asteroidea (class)		PredScav
		<i>Crossaster</i> sp. Müller & Troschel, 1840	PredScav
	Echinoidea (class)	Echinidea	PredScav
		<i>Echinocardium</i> sp. Gray, 1825	Dep
Annelida	Polychaeta (class)	Serpulidae Rafinesque, 1815	Susp
		<i>Arenicola marina</i> (Linnaeus, 1758)	Dep
Arthropoda	Decapoda (order)	Paguroidea Latreille, 1802	PredScav

### 2.5.3 Substrate

Several different types of substrate were registered from the video and images from the transects that hypothetically affect the distribution of brittle stars. These were fine sediment, coarse sediment, the presence of larger rocks, artificial substrate, and patches of accumulated macroalgae (Figure 9). The presence or absence of all these categories was registered for each image (Table 4).

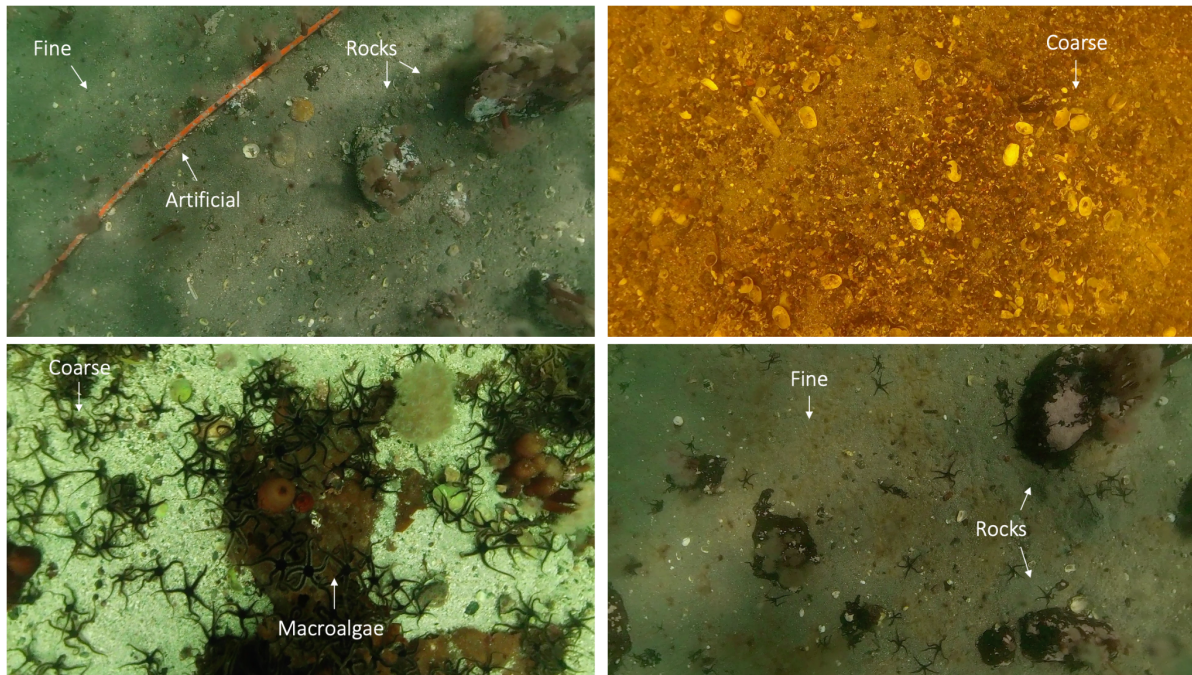


**Figure 9:** Examples of the different substrate categories that were registered as present/absent for every image: Fine sediment, coarse sediment, larger rocks, artificial substrate, and accumulation of macroalgae. Photo: Camilla Mult Marnor.

## 2.6 Multiple correspondence analysis (MCA)

A multiple correspondence analysis (MCA) was used to detect possible structures in the data set resulting from the image analysis. MCA is a type of multivariate analysis for summarizing and visualizing data containing more than two categorical variables. It is broadly used, especially for handling data from surveys. The analysis looks for the principal dimensions that explains the variability within the data (between the images) and identifies associations between the different variables. MCA also gives the relative importance of the different variables in explaining the variation in the data (Husson, 2016; Kassambara, 2017).

MCA was chosen as the appropriate analysis for this study due to the nature of the data: lack of quantitative variables due to lack of size reference. The software R (RStudio Team, 2022) was used for the statistical analysis. The MCA was performed on 356 images described by 12 variables: 3 numerical and 9 categorical. The different variables and the categories within the variables are listed in Table 4. The frequency of the different categories within each categorical variable is shown in Figure 10. The density category for *O. nigra* was set as a supplementary categorical variable, meaning that it did not contribute to the creation of the axes. Instead, it would be predicted by the other 8 active categorical variables (Kassambara, 2017).

Packages *FactoMineR* (Lê, Josse and Husson, 2008) and *Factoshiny* (Vaissie, Monge and Husson, 2021) were used for the statistical analysis. *Factoshiny* was also used for data visualization, together with the packages *tidyverse* (Wickham *et al.*, 2019) and *factoextra* (Kassambara and Mundt, 2020).

**Table 4:** The 12 variables that were used in the multiple correspondence analysis (MCA), 3 numerical and 9 categorical. The different categories are listed for categorical variables and the highest and lowest occurring values for numerical variables.

Variable	Type	Explanation	Categories / intervals
Location	Categorical	What transect line the image is from	Location1 Location2 Location3
Month	Categorical	Time of visit	May Sep Nov
Fine sediment	Categorical	Presence/absence of fine sediment in the image	Fine_y Fine_n
Coarse sediment	Categorical	Presence/absence of coarse sediment in the image	Coarse_y Coarse_n
Rocks	Categorical	Presence/absence of larger rocks in the image	Rocks_y Rocks_n
Artificial substrate	Categorical	Presence/absence of artificial substrate in the image (e.g., pipeline)	Artificial_y Artificial_n
Accumulation of macroalgae	Categorical	Presence/absence of patches of macroalgae in the image	Macroalgae_y Macroalgae_n
Feeding types	Categorical	Presence of other fauna categorized in functional groups based on feeding type (Table 3)	Dep PredScav Susp Dep_Susp PredScav_Susp Dep_PredScav_Susp Feeding_type_NA
Density <i>Ophiocomina nigra</i>	Categorical (supplementary)	A qualitative density category based on a subjective evaluation of coverage in each image (see Figure 8)	Absent Low Medium High
Depth	Numerical	Depth in meters measured by the ROV (distance from surface to top of ROV)	Min: 0.1 m Max: 8.2 m
<i>Ophiocomina nigra</i>	Numerical	Number of <i>O. nigra</i> registered in the image	Min: 0 Max: 631
<i>Ophiura</i> sp.	Numerical	Number of <i>Ophiura</i> sp. registered in the image	Min: 0 Max: 26

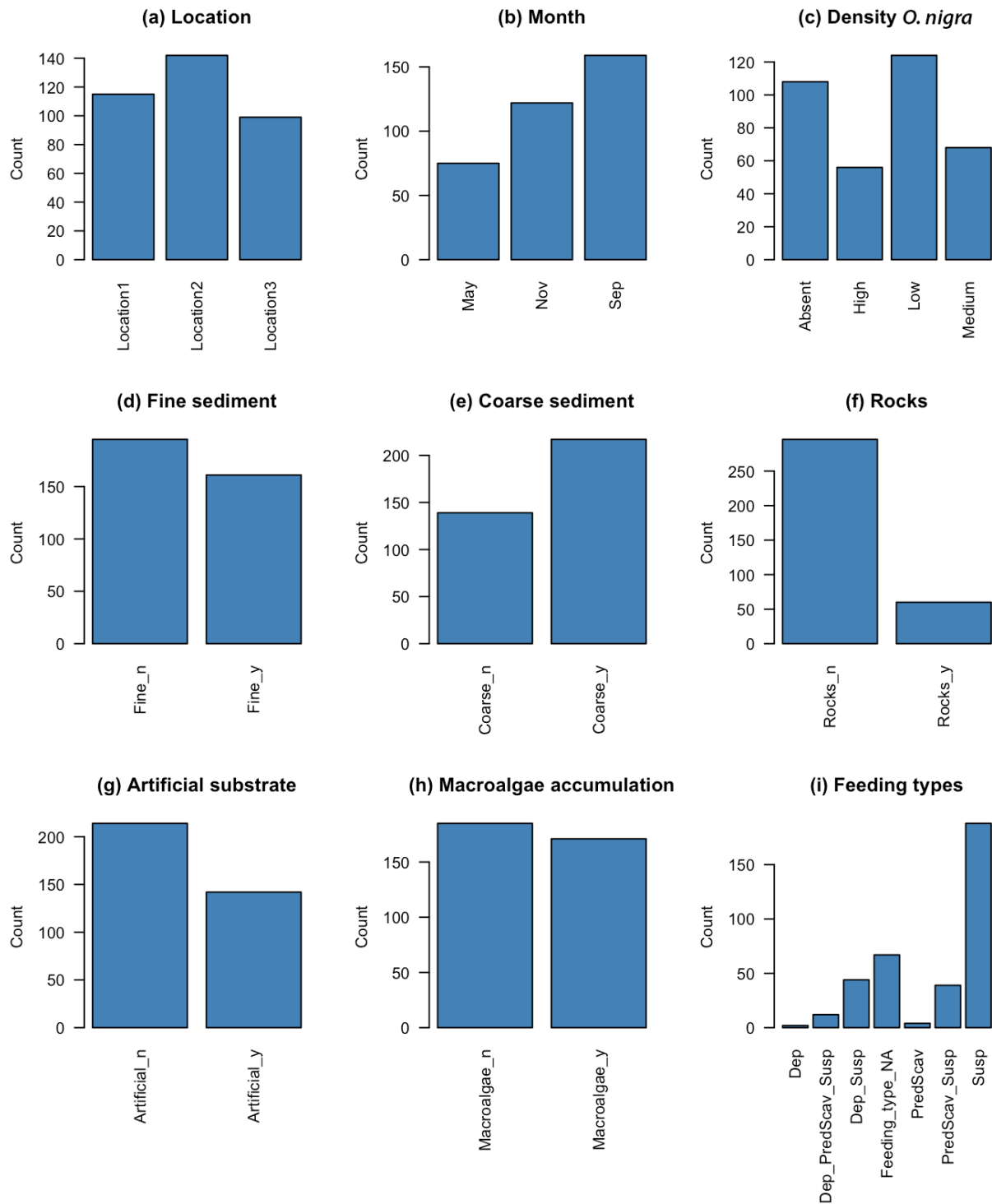


**Figure 10:** The frequency of the different categories within each categorical variable used in the multiple correspondence analysis (MCA): (a) location, (b) month of visit, (c) density category for *Ophiocomina nigra*, (d-h) categories related to substrate, (i) presence of other fauna categorized into functional groups based on feeding type.

## 2.7 Automatic identification of *Ophiocomina nigra*

Machine learning is a section of artificial intelligence (AI) which aims to imitate human learning by use of data and algorithms. It is largely used for prediction and classification (for details see Wang, Ma and Zhou (2009)). The algorithms require training data sets to learn from.

In the image analysis (see section 2.5) individuals of *O. nigra* were annotated with red dots. These images were used to train and test an algorithm for automatic classification and counting of *O. nigra*. A data set of 222 marked images and the unmarked originals of the same images was used. Images from Location 1 in May were excluded because another model of the 360 camera was used (Insta360 One X1, opposed to Insta360 One X2 for the rest of the surveys), as the algorithm will be trained for a specific camera model. Of the total number of images, 172 was used for training the algorithm. These images were flipped horizontally and vertically to multiply the training set by 4. A validation set of 19 images was used to evaluate how well the algorithm was training. The remaining 31 images that the algorithm had not seen were used for testing after training.

The automatic identification of *O. nigra* with machine learning and DDRNet (deep dual-resolution networks) (Hong *et al.*, 2015) was performed by Bjarne Kvæstad at SINTEF Ocean.

## 3 Results

### 3.1 Habitat description

#### 3.1.1 Location 1

The beginning of the transect was dominated by coarse sediment with small rocks and shells. Actinarians were widely distributed in patches. In May the actinarians had their tentacles expanded (Figure 11.A). In September and November a few had their tentacles expanded. Further out the substrate changed from small rocks to coarse sediment (shell sand). Actinarians were still highly abundant. In May *O. nigra* started to occur a bit out in the transect. In September and November *O. nigra* had high occurrence from early in the transect, in November already where the ROV was launched (Figure 11.D). The occurrence of *O. nigra* was generally high in this area. In some places they were aggregated at the base of actinarians (Figure 11). Patches of macroalgae occurred occasionally and *O. nigra* could be seen aggregated on kelp (Figure 11.B) but seemed to avoid filamentous algae. Nearing the end of the transect the seafloor was mainly dominated by *O. nigra* and some patches of macroalgae. Actinarians were almost absent at this point. Other fauna observed included gastropods, sea stars, hermit crabs, sea urchins and remains from sea urchin *Echinocardium*.

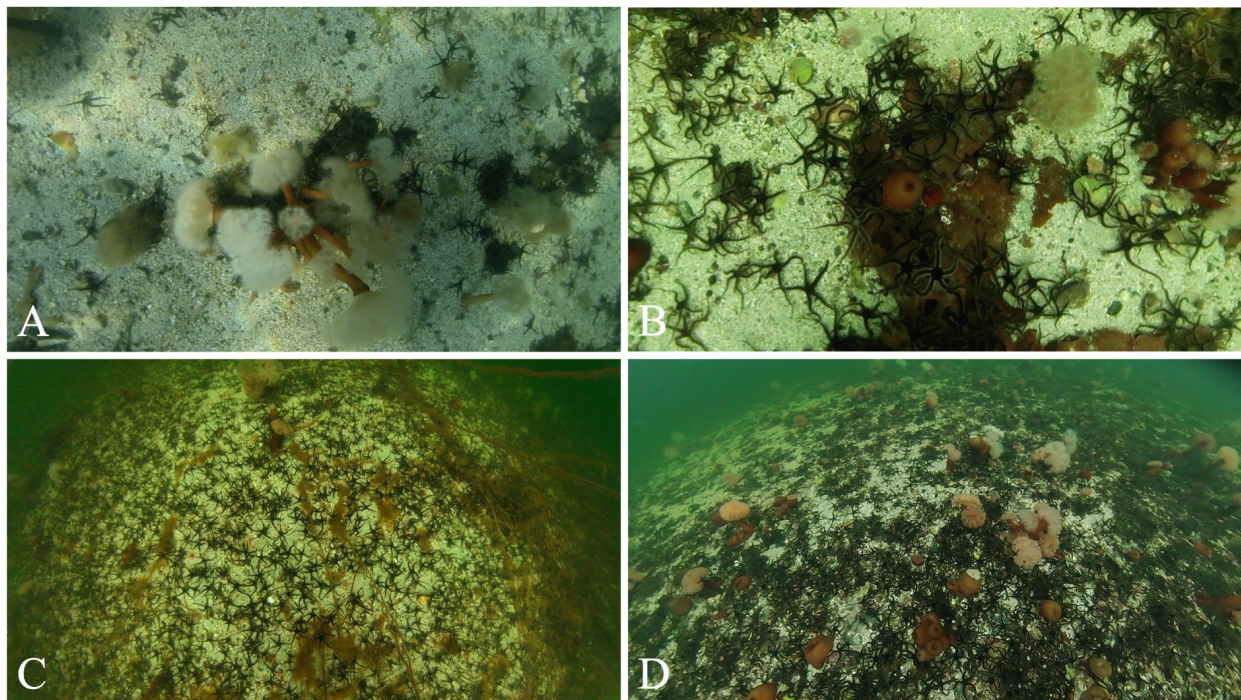


**Figure 11:** Frame grabs from Location 1: (A) Shell sand substrate and *Ophiocomina nigra* aggregated at the base of actinarians in May, (B) shell sand substrate and a patch of macroalgae crowded by *O. nigra* in November, (C) example of a high occurrence of *O. nigra* in this area and filamentous algae in September, (D) high density of *O. nigra* together with actinarians shortly after launching the ROV in November.

### 3.1.2 Location 2

The transect was along a pipeline on the seabed from the shore and out. In the very beginning the substrate consisted of coarse sediments with small rocks, shells, and remains from the sea urchin *Echinocardium*. After a short distance the substrate changed to fine sediment. Actinarians (including *Metridium senile* (Linnaeus, 1761)) was highly abundant on the pipeline. In May all had their tentacles expanded, and large areas of the pipe were covered (Figure 12 A, C). In September and November most actinarians had their tentacles withdrawn. Patches of accumulated macroalgae occurred next to the pipe (Figure 12 B, C). Piles and holes were observed in the fine sediment, assumed to be traces of *Arenicola marina*. *Ophiura* sp. was first observed at approximately 2.5 m depth (May). However, they were well camouflaged, and some partly covered by sediment. Therefore, individuals might have been overlooked. There were relatively many of them in some places but compared to the density category of *O. nigra* it would have been categorized as low to medium density. The *Ophiura* were of varying size (Figure 12 D, Figure 19). *Ophiocomina nigra* occurred mainly related to patches of macroalgae, on the pipeline, and on rocks (Figure 12 B). It could be challenging to see and count exact numbers of *O. nigra* due to shadows and the dark color of the macroalgae in combination with the dark color of *O. nigra*, and in May due to the cover of the tentacles of actinarians. Additional fauna observed was sea urchins, *Crossaster* sp., bivalves, Cerianthidae, gastropods, a flounder, and red calcareous algae.

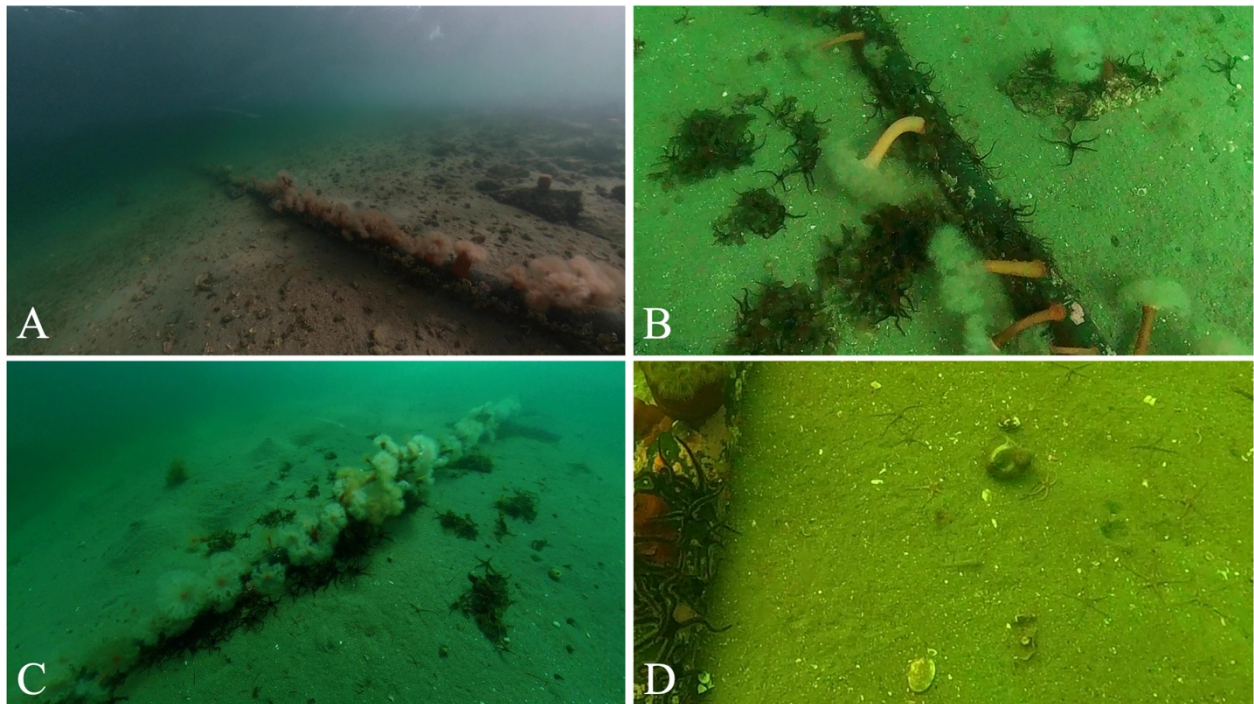


**Figure 12:** Frame grabs from Location 2: (A) coarse substrate with more rocks at the beginning of the transect, from May, (B) substrate preference of *Ophiocomina nigra* for the hard substrates of the pipeline and a rock and aggregations on patches of macroalgae, from May, (C) pipeline covered by the tentacles of actinarians in May, (D) many *Ophiura* sp. on the fine sediments next to the pipeline and *O. nigra* on the pipeline in September.

### 3.1.3 Location 3

Location 3 had coarse sediments at the beginning of the transect with small rocks, remains from shells and patches of actinarians (Figure 13.A). The sediment then changed to a finer sediment, but it was still categorized as coarse sediment. Larger rocks with actinarians occurred (Figure 13.B). Artificial substrate occurred as a small orange pipe (Figure 13.C) and several cords. In May *O. nigra* was mainly aggregated on rocks (Figure 13.B) and could be difficult to see due to shadows and expanded tentacles of actinarians. In September *O. nigra* also occurred on the sediments (Figure 13.C). In November *O. nigra* occurred closer to the shore and aggregated on rocks (Figure 13.D). Occurrence of *O. nigra* increased further out in the transect. Some *Ophiura* sp. were observed in September, one in May, and none in November. They were more difficult to detect as they were camouflaged on the substrate. Filamentous algae were observed mainly in September. Other fauna observed included sea urchins, Cerianthidae and bivalves.

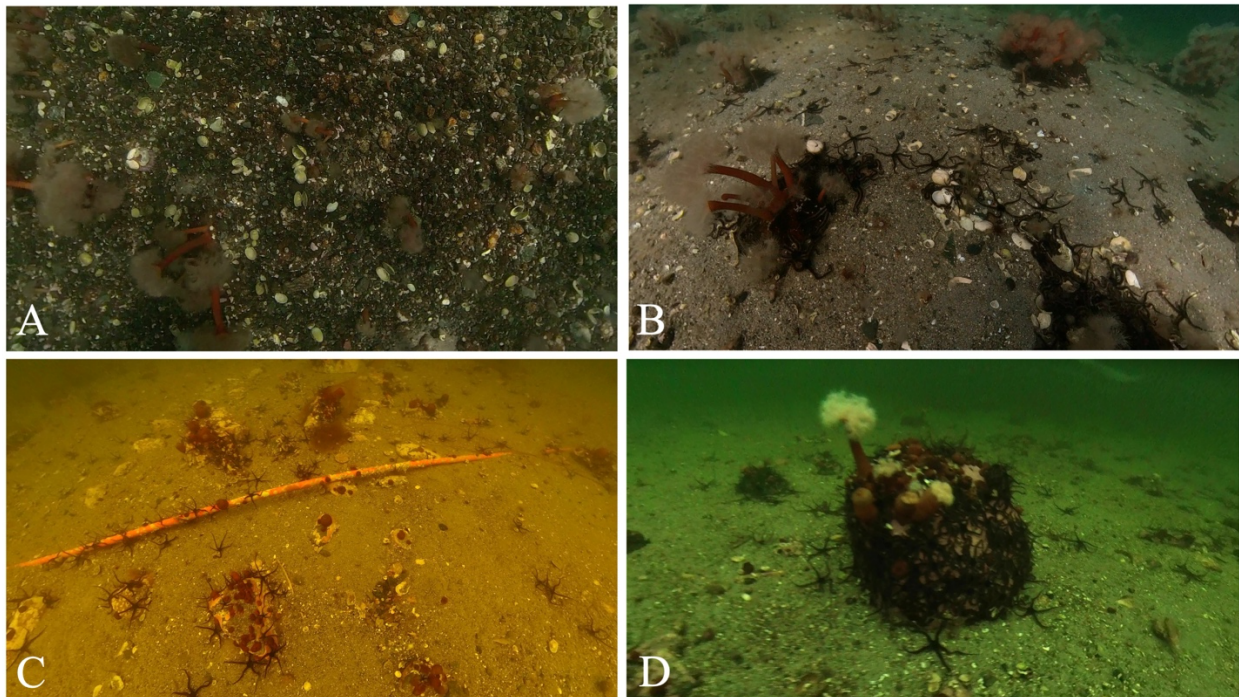


**Figure 13:** Frame grabs from Location 3: (A) Coarse sediment at the beginning of the transect with small rocks, shells and actinarians, from May, (B) coarse sediments with shells, actinarians and *Ophiocomina nigra* patchily distributed, from May, (C) artificial substrate (orange pipe) and coarse sediments with rocks and *O. nigra*, from September, (D) a rock covered by *O. nigra* and actinarians, from November.

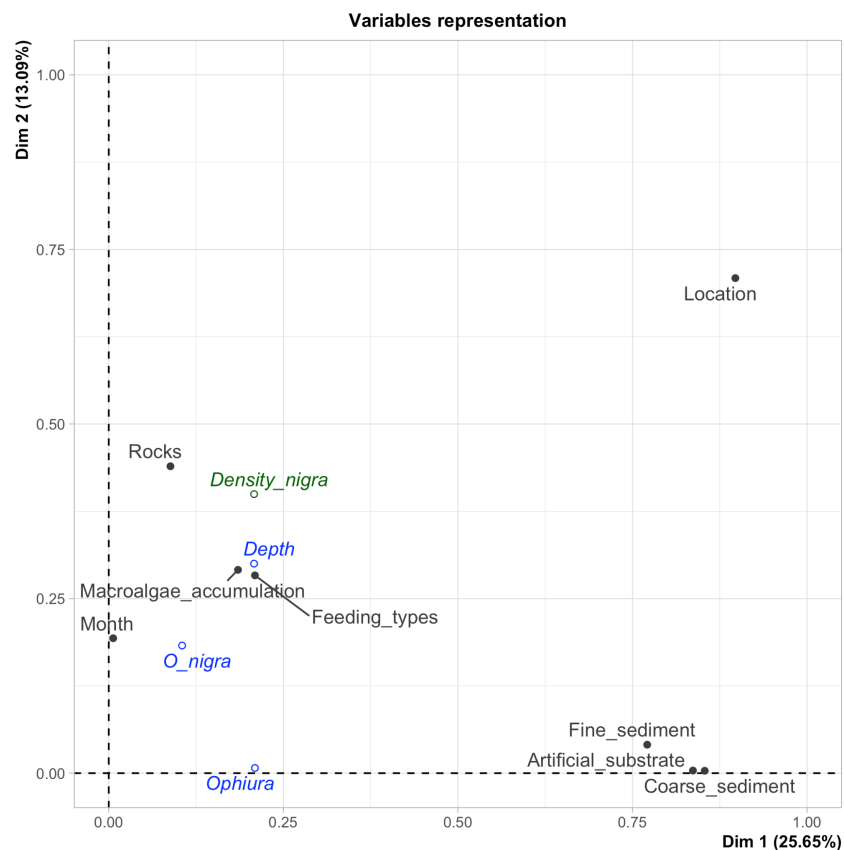


## 3.2 Multiple correspondence analysis (MCA)

The MCA creates dimensions that combined account for all the variation in the data set (Table 4). The first two dimensions account for the highest percentage of the variation in the data set compared to any other two dimensions. Thereby, they are the only dimensions discussed in this context and will be referred to as the principal dimensions. The principal dimensions described 38.7 % of the total variance in the data set, 25.6 % by dimension 1 (Dim1) and 13.1% by dimension 2 (Dim2).

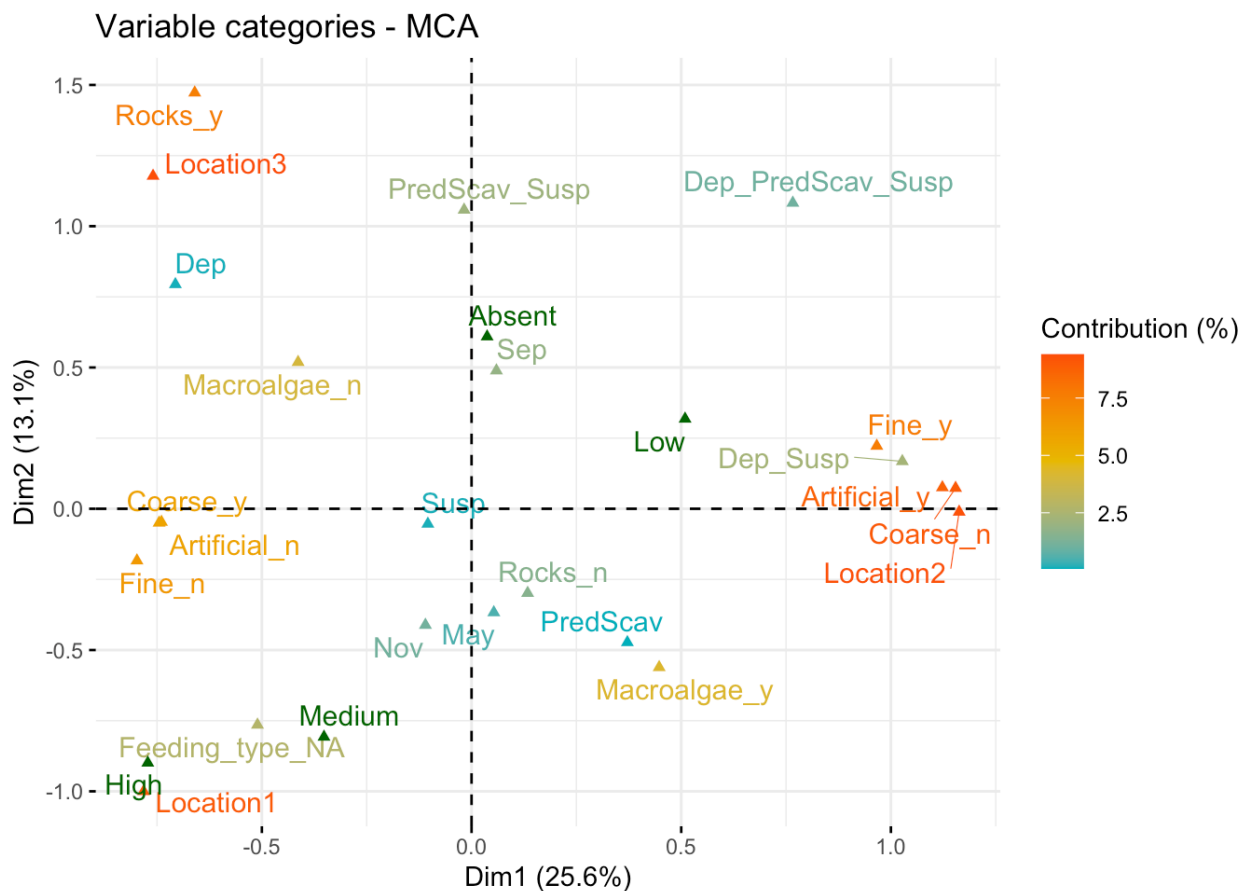
### 3.2.1 Contribution of variables

Figure 14 shows the correlation between the different variables and the principal dimensions. For Dim1 fine sediment, artificial substrate, coarse sediment, and location was of highest importance. For Dim2 location was of high importance. Rocks, macroalgae accumulation and feeding types were of intermediate importance. Month was of low importance.



**Figure 14:** The absolute representation of the variables included in the multiple correspondence analysis (MCA) in relation to the principal dimensions (Dim1 and Dim2). The coordinates are the squared correlations between the dimensions and the variables. The active categorical variables are in gray, the supplementary categorical variable in green, and numerical variables in blue.

Figure 15 shows the strength (%) and direction of the contribution of the different variables in building the principal dimensions, and the supplementary categorical variable (Density *O. nigra*). For Dim1, the presence of artificial substrate, presence of fine sediment/absence of coarse sediment and location 2 were of high positive influence. The presence of deposit feeders together with suspensions feeders were positively correlated with Dim1 but had a relatively low contribution in the making of the dimensions. The presence of coarse sediment/absence of fine sediment and artificial substrate had a high contribution in the negative direction. The presence of rocks was a variable of high contribution to the principal dimensions, in the negative direction for Dim 1 and positive direction for Dim 2. The absence of rocks was however not very defining. Feeding types and month had a low contribution.



**Figure 15:** Contribution of variable categories in the multiple correspondence analysis (MCA) in defining the principal dimensions (Dim1 and Dim2). The variable categories are colored according to their contribution in percent. The categories of the supplementary categorical variable (density of *Ophiocomina nigra*) are shown in dark green.

### 3.2.2 Distribution of samples within the different variables

The distribution of the samples (images) in relation to the different active categorical variables, and the supplementary categorical variable (density of *O. nigra*) is shown in Figure 16. The locations are well separated when looking at the principal dimensions and their contributions are high (Figure 16.a). The distribution of the samples for Month (Figure 16 b) supports the interpretation of its low influence from Figure 14: the points are scattered, the confidence ellipses are all positioned close to the origin, and the confidence ellipses for May and November are overlapping, indicating that these two variable categories are not significantly different.

The density category for *O. nigra* (Figure 16 c) shows that medium and high density is concentrated in the lower left corner (negative end of Dim1 and Dim2), which is the same position as Location 1 in Figure 16 a. The categories within the variables fine sediment, coarse sediment and artificial substrate are well separated by Dim1 (Figure 16 d, e, g). The macroalgae categories was separated by Dim2 (Figure 16 h). The presence of rocks had a lower frequency than the absence of rocks (Figure 16 f) which supports its higher contribution to the principal dimensions (Figure 15). The categories for different combinations of feeding types are scattered (Figure 16 i). Only 4 samples had *PredScav*, giving this category a very large confidence ellipse, and only 2 samples had *Dep*, resulting in a line instead of a confidence ellipse.

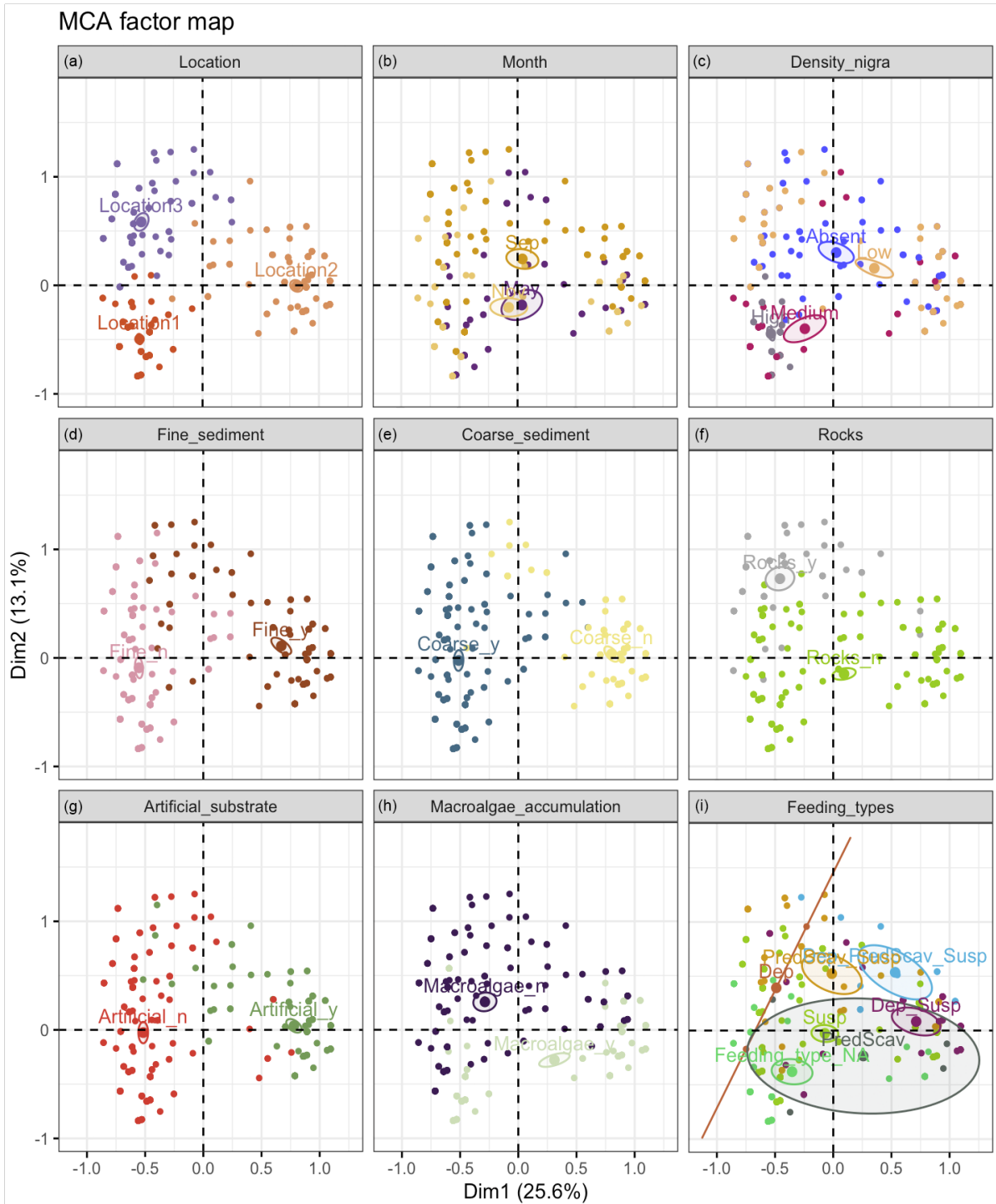


**Figure 16:** Multiple correspondence analysis (MCA) factor map. The distribution of the samples in relation to the different categorical variables (described in section 2.6): (a) the different locations, (b) month of visit, (c) qualitative density category of *Ophiocolina nigra*, (d-h) presence/absence of fine sediment, coarse sediment, large rocks, artificial substrate and macroalgae, (i) presence of other fauna based on their feeding types.

### 3.2.3 The spatial distribution and density of *Ophiocomina nigra* related to the categorical variables

The MCA biplot (Figure 17) combines the results shown in Figure 15 and Figure 16 c. It is a point cloud made from the samples, the variable categories, and the supplementary categorical variable (density *O. nigra*) that is predicted by the other categorical variables. The three locations are located far away from each other, indicating that they were distinctly different from each other. This is supported by Figure 16 a where the samples for the locations are almost entirely isolated from each other.

The MCA indicates correlations between Location 1 and coarse sediments, absence of other fauna, and medium to high density of *O. nigra*. There is a possible correlation between the occurrence of macroalgae and higher densities of *O. nigra* (see in Figure 16 h where many of the samples for presence of macroalgae is in the same area as the samples for Location 1 in Figure 16 a).

Location 2 showed high correlation with artificial substrate, which was due to the pipeline that the transect was following. The MCA confirmed a high correlation with fine sediments in this location and showed correlation with deposit feeders and suspension feeders, however these variable categories had a low contribution to the principal dimensions (Figure 15).

Location 3 was correlated with presence of larger rocks, and this was a highly defining category according to Figure 15.

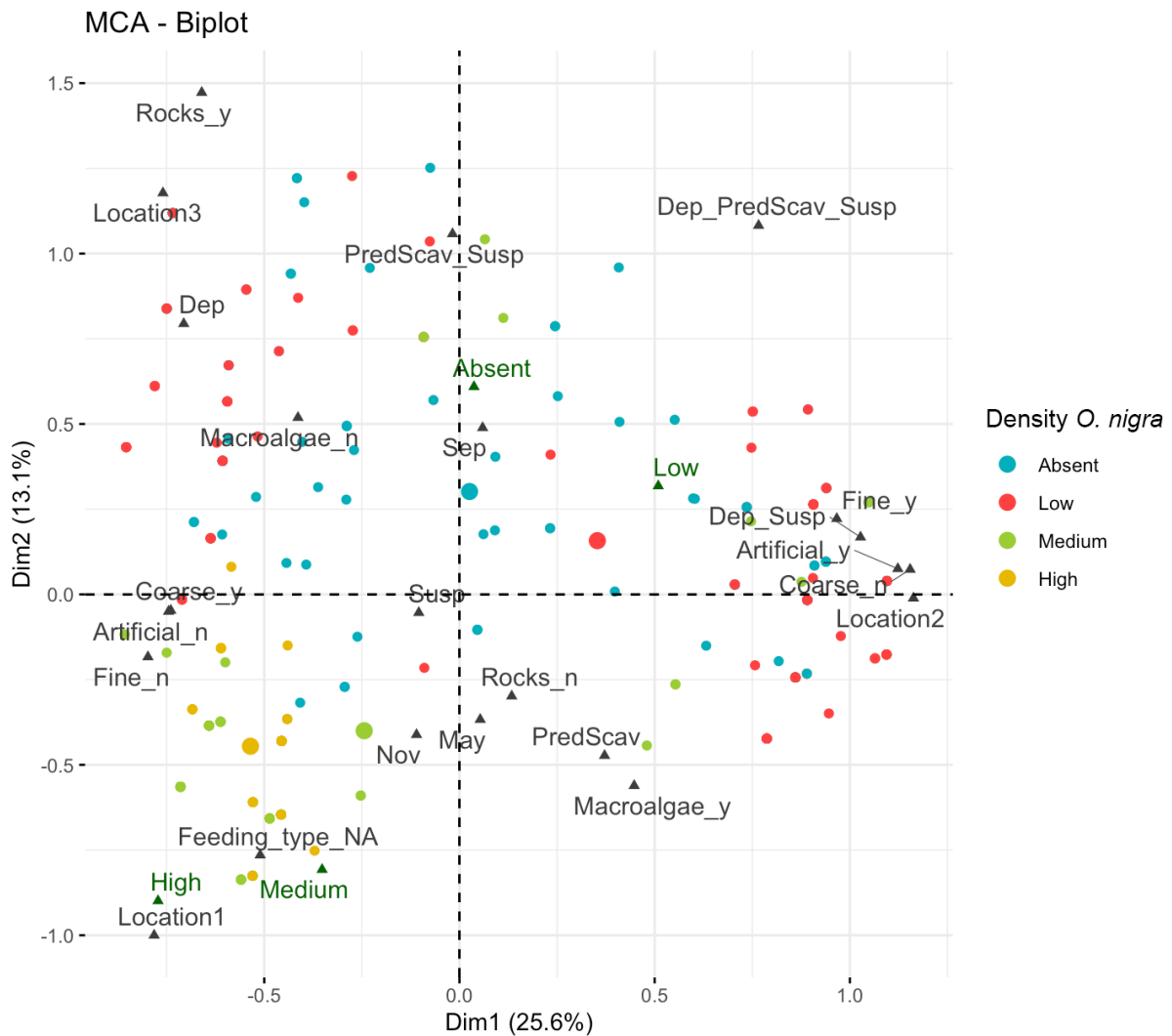


**Figure 17:** Multiple correspondence analysis (MCA) biplot. All categories from the categorical variables (e.g., “Rocks\_n” and “Rocks\_y” for absence and presence of larger rocks in the samples (images)) and the samples related to the principal dimensions (Dim 1 and Dim2). The categories of the supplementary categorical variable (density of *Ophiocomina nigra*) are predicted by the other variables and are shown in dark green. The samples are colored according to the density classification of *O. nigra* for that sample (absent, low, medium, high).

### 3.2.4 The numerical variables related to the dimensions of the multiple correspondence analysis (MCA)

Numerical variables are not used to build the dimensions of the MCA, but they can be plotted on the dimensions to see their directions in relation to the dimensions (Figure 18). The numerical variable for *O. nigra* is directed towards the bottom left/negative values for both principal dimensions. This supports the interpretation of the biplot and the prediction of the density category for *O. nigra* based on the categorical variables (Figure 16 c, Figure 17). The numbers of *Ophiura* are negatively correlated with *O. nigra* and is pointed in the same direction as Location 2 (Figure 17), which was the location where most *Ophiura* were found, in addition to the variables fine sediment and artificial substrate (the pipeline in Location 2). Depth is

almost 90 degrees on the other two numerical variables, meaning that depth was of little importance for the occurrence of ophiuroids in this data set, supporting the interpretation of Figure 14.

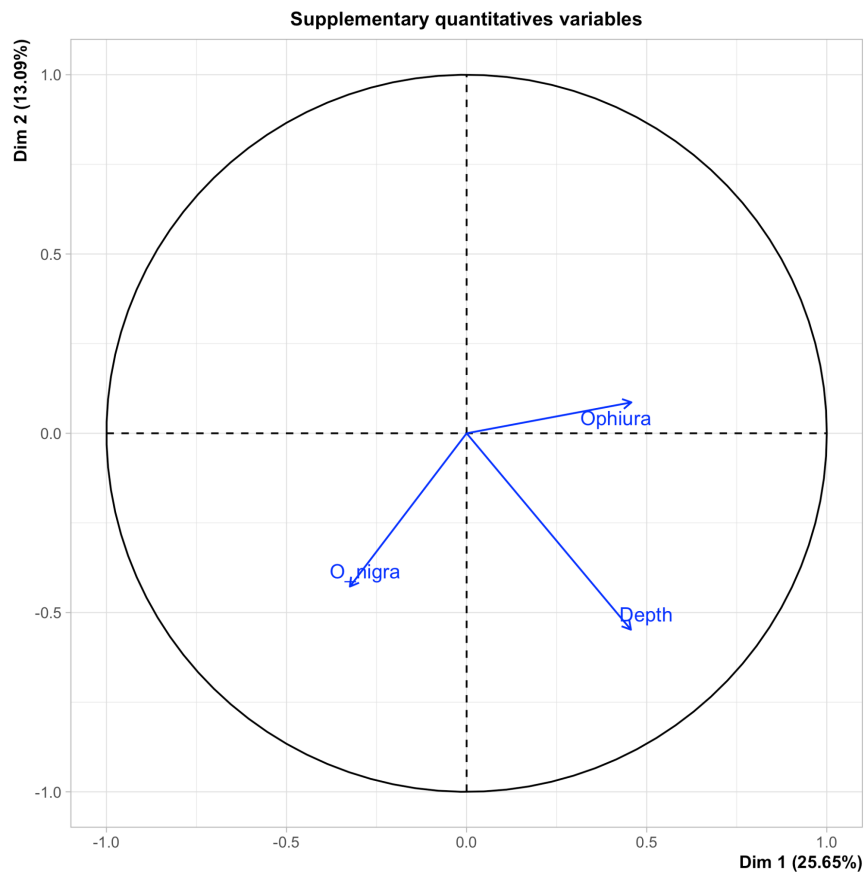


**Figure 18:** The numerical variables “Depth” and numbers of *Ophiocomina nigra* and *Ophiura* sp. plotted on the principal dimensions (Dim1 and Dim2) from the multiple correspondence analysis (MCA) to show their direction related to the dimensions.

### 3.3 Automatic identification with machine learning

The performance of the algorithm used for automatic identification of *O. nigra* with machine learning was an accuracy of 86.7%. This was based on the number of individuals identified in the 31 images for testing by human detection versus the numbers automatically identified by the algorithm. The accuracy evaluation was solely based on a comparison of numbers and did not consider the occurrence of false positives and/or negatives or if the algorithm counted the same individuals as was registered by a human. The algorithm avoided confusion between *O. nigra* and *Ophiura* sp. (Figure 19). Figure 20 shows additional two examples from the testing of the performance of the algorithm, one where the count was higher from the human (A), and one where the count from the algorithm was higher (B).

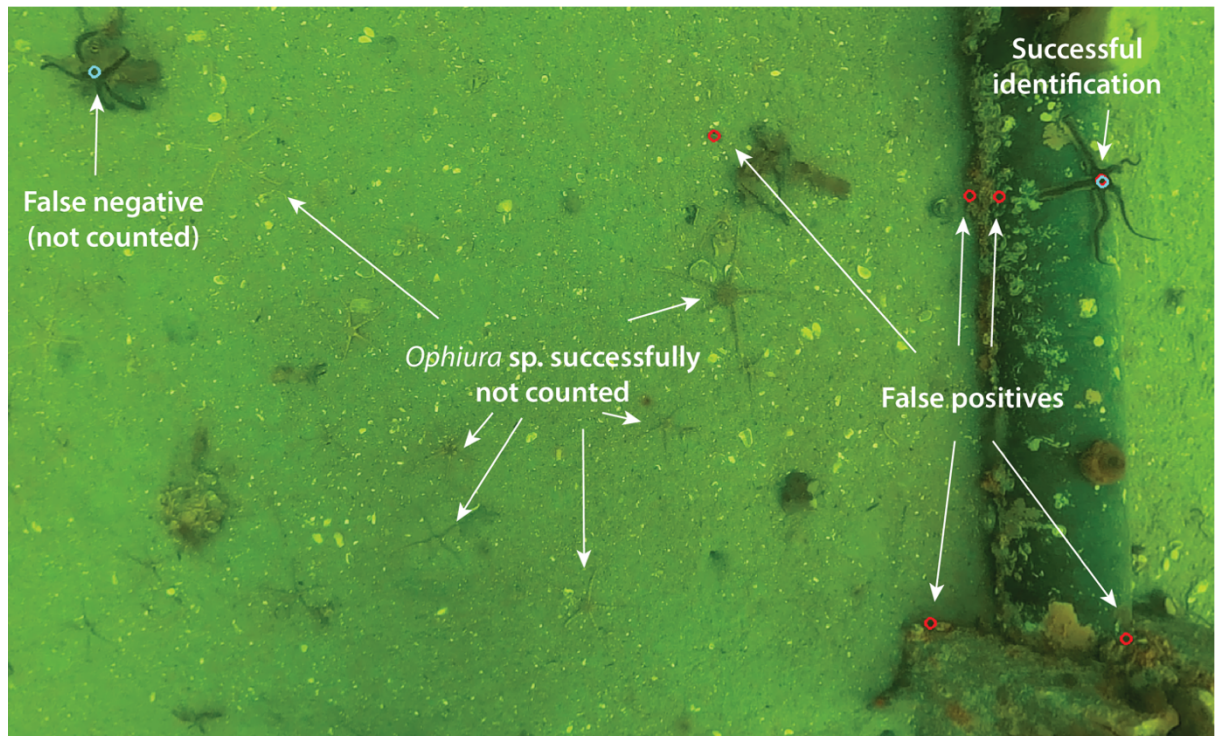


**Figure 19:** Example of potential for improvement of the algorithm that were used for automatic identification of *Ophiocomina nigra*. Identification performed by marine biologist (blue) and identification performed by the algorithm (red). The algorithm has successfully not counted *Ophiura* individuals, but there are several false positive counts of *O. nigra*. One out of two *O. nigra* is not counted.



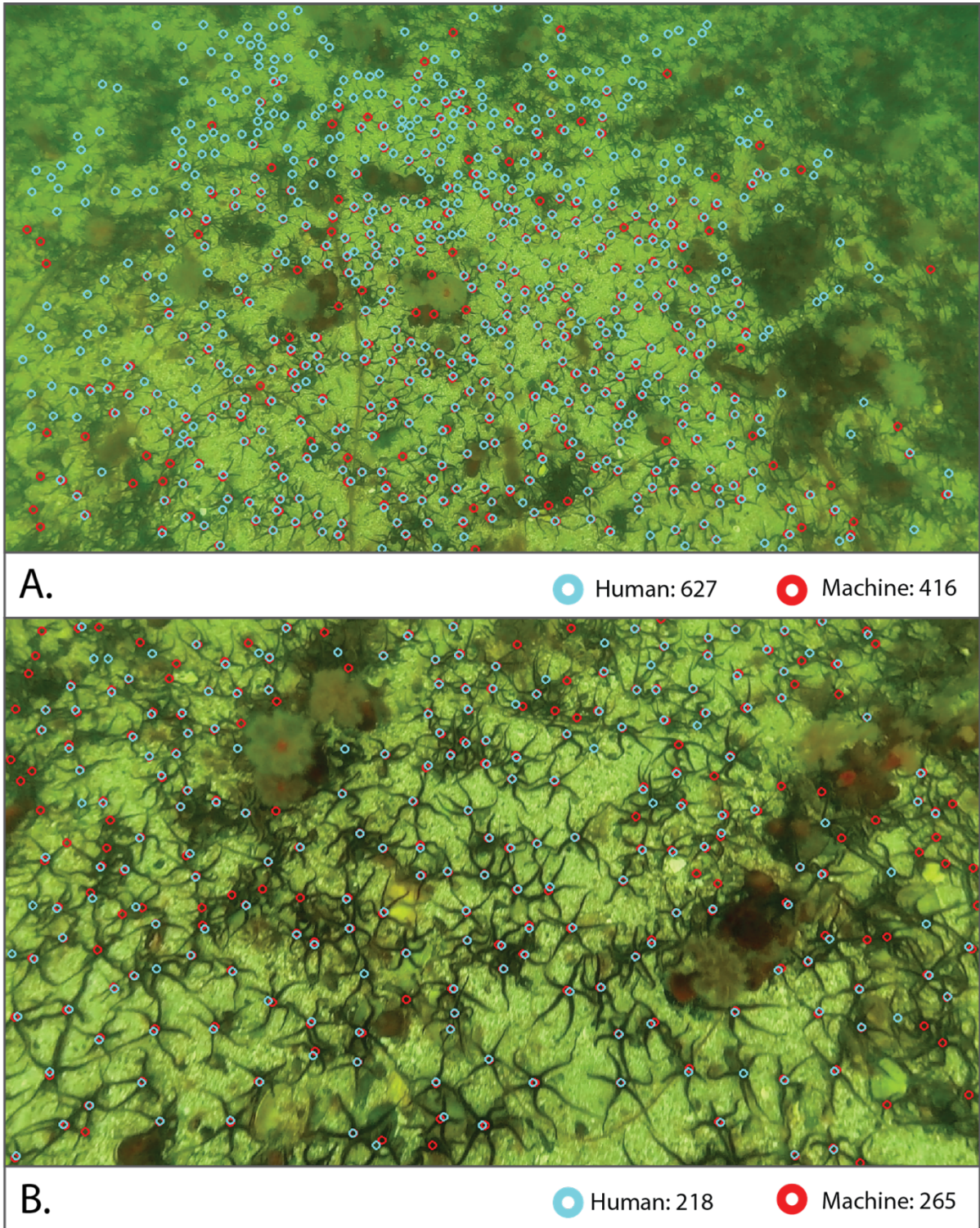


**Figure 20:** Examples of images where individuals of *Ophiocomina nigra* have been automatically identified by a machine learning algorithm, performed by Bjarne Kvæstad (section 2.7). The identification performed by the algorithm is in red and by a marine biologist in blue.

## 4 Discussion

360 video from the transects showed what appeared to be three rather different habitats. This observation was confirmed by the multiple correspondence analysis (MCA) where the location was the most defining variable. Variables related to the substrate were also of high importance for describing the variation in the data set. One brittle star bed with *Ophiocomina nigra* was found in Location 1 on coarse sediment. Other visible fauna was scarce in this area. Apart from the brittle star bed, *O. nigra* seemingly preferred hard and elevated surfaces, and patches of macroalgae. *Ophiura* sp. was mainly found in Location 2 on fine sediment.

The 360 camera mounted in front of the ROV turned out to be a useful tool for assessing different benthic habitats and the spatial distribution of brittle stars in shallow areas. Any seasonal variation of importance was not detected with the method. Automatic identification of *O. nigra* with machine learning showed promising results with an accuracy of 86.7% based on the number counted by the algorithm compared to what was counted manually.

### 4.1 Assessing the spatial distribution of brittle stars

#### 4.1.1 *Ophiocomina nigra* brittle star bed

Out of the three locations visited in Hopavågen, Location 1 held the highest numbers of *Ophiocomina nigra*. In this location *O. nigra* was dominating the visible benthic fauna in all three seasons and the area can be categorized as a brittle star bed (Hughes, 1998). Location 1 was the transect closest to Straumen. Since Hopavågen is narrower in this area and Straumen is the only connection to the fjord, with large water masses moving in and out with the tide (Marion, 1996), this location is more exposed to currents than the other two. Brittle star beds of *O. nigra* and/or *O. fragilis* occur in areas with strong to weak tidal streams (Hughes, 1998). However, one can presume that moderate current conditions are favorable, transporting more seston over the brittle star beds. Warner (1971) suggested that the aggregating behavior of *O. fragilis* give them the ability to inhabit areas with stronger currents, which facilitates their suspension feeding activity. *Ophiocomina nigra* is a more flexible feeder than *O. fragilis* (Blanchet-Aurigny *et al.*, 2015), but it is feasible to assume that this species can gain the same benefits from this behavior, and that the aggregated population in Location 1 has seston as an important food source.

Location 1 additionally supported a high abundance of actinarians, which were also present in the other two locations. The occurrence and behavior of actinarians can give indications on the hydrodynamic conditions and presence of food in the water masses. For instance, *Metridium senile* eats zooplankton (Sebens and Koehl, 1984), and tentacle expansion is positively correlated with increased currents, and the interaction between currents and food availability (Robbins and Shick, 1980). In May actinarians had their tentacles expanded in all three locations, which might indicate that the conditions were favorable for suspension feeding during this visit. *Ophiocomina nigra* and *M. senile* might be competitors for food, but *O. nigra* is able to exploit other food sources as well and have the mobility to move to better areas.

Nevertheless, *O. nigra* was observed to frequently be located at the base of actinarians which indicates that this is not a disadvantage for their access to food.

Brittle star beds have been observed to be a rather stable phenomenon (Aronson, 1989; Hughes, 1998), apart from some exceptions (mass mortality of *Ophiothrix quinquemaculata* (Delle Chiaje, 1828) in the Gulf of Trieste (Stachowitsch, 1984), and near disappearance of *O. fragilis* and *O. nigra* in the Bay of Douarnenez (Guillou, Blanchet-Aurigny and Le Goaster, 2013)). This seems to be the case in Hopavågen as well. Teacă, Ungureanu and Mureşan (2017) described a dense assemblage of *O. nigra* in what was the beginning of the transect in Location 1 in this study, observations done in May 2012 and August 2013. They observed that the occurrence was stable from the first to second visit, and that the species seemingly was unaffected by food limitation or changes in temperature between the seasons (Teacă, Ungureanu and Mureşan, 2017).

Predation has been suggested to be an important biotic variable to limit the distribution of brittle star beds (Hughes, 1998). Known predators of brittle stars include crabs, sea stars and fish (Aronson, 1989; Guillou, Blanchet-Aurigny and Le Goaster, 2013). Aronson (1989) showed that *O. fragilis* and *O. nigra* were more prone to predation on rocky reef communities than in brittle star beds. Crabs and fish were responsible for most of the attacks in the rocky reef communities. The sea star *Asterias rubens* had about the same number of attacks in both habitat types. However, they are slow eaters (8-24 hours to consume a brittle star in the laboratory), so they are not expected to affect a brittle star bed unless they occur in very large numbers (Aronson, 1989). High numbers of several sea star species were probably the explanation for the near disappearance of *O. fragilis* and *O. nigra* in the Bay of Douarnenez, France, in the 1980s (Guillou, Blanchet-Aurigny and Le Goaster, 2013). Some sea stars were observed in the brittle star bed in Location 1. Fish were also occasionally observed during the surveys. One can assume that the predation pressure on the brittle star bed in Hopavågen is relatively small considering its persistence.

#### **4.1.1.1 Brittle star beds and other fauna**

For the image analysis, the surrounding fauna was divided into functional groups based on their main feeding strategy, as this could possibly indicate what types of food that was present. High and medium density of *O. nigra* was correlated with the absence of other fauna (*Feeding\_type\_NA*) (Figure 17). This indicates that where the density of *O. nigra* was high, there was little room for other fauna, at least macrofauna that was detectible with this method. Aronson (1989) low species diversity in brittle star beds in the British Isles, both in brittle star beds dominated by *O. nigra* and *O. fragilis* respectively. According to Hughes (1998) aggregations of brittle stars tend to exclude other epifauna on bedrock but there is often a rich fauna under the brittle star beds on sedimentary substrata. As no physical samples were collected in this study, it is not possible to say anything about epifauna and infauna under the brittle star, and it is not possible to collect such information with this method.

#### 4.1.2 *Ophiocomina nigra* on macroalgae and hard substrate

Apart from in the brittle star bed in Location 1 *O. nigra* seemingly preferred hard substrate as this species was observed to be aggregated on the pipeline and on larger rocks in Location 2 and 3 respectively (Figure 12 B, Figure 13 D). The explanation for this might be that the species use higher areas to get access to more food particles drifting by in the water column. The pipeline created a hard substrate in an area with fine sediments, posing as suitable substrate for actinarians and *O. nigra*. The pipeline might also pose as a physical barrier, hindering objects on and close to the seafloor to pass with the currents. This might be the reason for the presence of patches of macroalgae along the pipeline.

*Ophiocomina nigra* was observed aggregated on these patches of macroalgae (Figure 12 B), and occasionally on patches of macroalgae in Location 1 (Figure 11 B). Taylor (1958) examined gut contents of *O. nigra* and found sessile algae to be a part of the species' diet, especially for individuals living in inshore areas (Taylor, 1958, as discussed by Fontaine, 1965). Mortensen (1924) also described *O. nigra* climbing Laminarian macroalgae, and that they eat the macroalgae and small animals on the macroalgae. The position of brittle stars related to macroalgae was not specifically registered in the image analysis; it was only registered if macroalgae was present or absent in the individual images. This may have influenced the correlation between the occurrence of macroalgae and *O. nigra* in the results from the MCA, where the presence of macroalgae was of intermediate importance for the variation in the data set (Figure 15), and the correlation between presence of macroalgae and *O. nigra* was not evident from the results of the MCA (Figure 17).

#### 4.1.3 Spatial distribution of *Ophiura* sp.

Brittle stars of *Ophiura* sp. were mainly observed in Location 2, with a few observations in the other two locations. These observations were supported by the results of the image analysis and the MCA, where the numerical variable of *Ophiura* sp. was pointed in the same direction (Figure 18) as Location 2 (Figure 17). These brittle stars were well camouflaged in the fine sediment and was not seen while driving the ROV but was visible in the video from the 360 camera. However, as they were hard to see, their numbers were most likely underestimated in some images.

According to the MCA, Location 2 was correlated with fine sediment, artificial substrate (the pipeline), deposit feeders, suspension feeders, and a low density of *O. nigra* (Figure 17). The numerical variables also showed a negative correlation between numbers of *Ophiura* sp. and numbers of *O. nigra* (Figure 18). This indicates that the species have different preferences, which was supported by observations from the video and images from Location 2: *Ophiocomina nigra* was mainly positioned on the pipeline, rocks, and patches of macroalgae while *Ophiura* sp. was observed on the fine sediment (Figure 12 B and D). Boos *et al.* (2010) found that *O. albida* preferred fine over coarse sediment, while *O. ophiura* did not show any preference. They observed *O. albida* to exhibit stationary burrowing behavior, which they suggested to be associated with deposit feeding and predation/scavenging on infauna, while *O. ophiura* hunted actively for epibenthic prey (Boos *et al.*, 2010). The correlation with deposit

feeders in Location 2, which was remains of *Echinocardium* (Figure 12 D) and characteristic traces in the sediments (holes and casts) from *Arenicola marina* (Riisgård and Banta, 1998), can indicate that the fine sediment in this area was suitable for deposit feeding.

#### **4.1.4 The distribution of brittle stars in relation to temperature and depth**

The ROV measured the depth of the ROV and the water temperature, and this was registered for each of the images used in the image analysis. The variation in temperature was low within each visit and between the different locations. The largest variation in temperature was between the different months (roughly up 6°C from May to September and down 6-9°C from September to November). Thus, the different months included in the analysis also indicates different temperatures and temperature as a numerical variable was not included in the MCA. Since *Month* was of low importance for describing the variability in the data set (Figure 14), it is reasonable to conclude that temperature was not a determining factor in this case. According to the MCA, depth was also of low importance (Figure 18). However, only shallow areas were investigated, and the depth interval was small (maximum depth of the ROV registered was 8.2 m). It is possible that depth is of importance for the distribution of brittle stars on a larger spatial scale and depth interval, potentially in combination with other variables (e.g., as was found by Piepenburg (2000) for Arctic brittle stars).

## **4.2 Factors influencing video and image quality**

### **4.2.1 Field of view (FOV)**

With the 360 camera comes new considerations regarding choice of orientation and field of view (FOV) for images for the image analysis. Opposed to normal video, one must choose where in the 360 globe the edited video should “look”, and the size of FOV (zoomed in/out), that together with altitude determines the size of the area of seafloor covered by each image. Since the focus of this study was benthic organisms, an orientation showing the seafloor directly from above (i.e., zenith view) was chosen. The size of FOV is chosen by zooming in or out. When zooming in as much as possible, a great deal of information is lost since the image will only cover a relatively small area on the seafloor compared to what is available with the tool. As you zoom out, more and more distortion in the edges will occur due to barrel distortion (Park, Byun and Lee, 2009). With a smaller FOV you can capture more details which can be useful for identification. A larger FOV gives an overview of the habitat, composition of species and a context, but less details (Funk, Bryant and Heckman Jr, 1972) as the number of pixels per area of seafloor covered by the image is reduced (i.e., lower spatial resolution). A FOV that aimed to be an intermediate solution between these trade-offs were chosen for this study (Figure 7, blue frame). In some images the distortion was helpful as it was possible to see the raised arms of *O. nigra* from the side and sometimes individuals were easier to see in that way than directly from above. However, the distorted edges of the images posed a challenge for image analysis in most cases and many individuals of *O. nigra* in the edges of the images were not counted because it was not possible to distinguish between individuals or to be certain about the identification. Distortion will be a challenge with fisheye lenses (Park, Byun and Lee, 2009)

and how to account for this must be considered related to the goal and requirements for the study.

#### **4.2.2 Settings for video resolution**

The 360 camera has several options for video resolution (Table 2). Higher spatial resolution gives lower options for frames per second (fps). Fps indicates how many image frames each second of the video consists of. A higher frame rate preserves detail sharpness when there is more motion (i.e., reduce motion blur) and gives more options when editing, e.g., slow motion possibilities. The spatial resolution (5.7K, 4K, 3K) indicates the number of pixels on the photosensor and the number of pixels displayed in the image or video (GoPro, 2021). A higher number of smaller pixels will give the possibility to distinguish more details in the images and video (i.e., higher spatial resolution) which is an advantage for taxonomic classification. By reducing the number of pixels, the size of each pixel increases and can capture more light, increasing the sensitivity of the sensor, increasing image quality in low-light conditions. Thus, there is a trade-off between spatial resolution and sensitivity. In November many images from the transects were blurry. This was possibly due to cloudy conditions and in general reduced ambient light in this time of year, and a lower speed of the ROV would have been required to get images of the same quality as the other visits with the same video settings. For the detail level required for this study, most of the images were still possible to use, but for a study purpose requiring a higher detail level this would have been serious for the data/outcome. A possible solution could have been to increase fps from 30 to 50 (67% increase). However, this would require a change in spatial resolution from 5.7K (16.6 MP (megapixels)) to 4K (7.4 MP), giving 55% reduction in pixel number. How this would have affected the results, and what is the best option for this study would have to be further investigated.

#### **4.2.3 The effect of a three-dimensional seascape**

One challenge with optical methods that record the seascape from a zenith perspective is the three-dimensional structure of the seascape and its components. Actinarians were common in all three transects. In May most actinarians had their tentacles expanded which covered up an area around them (e.g., Figure 11 A, Figure 12 A and C). This posed a challenge in all three transects and many *O. nigra* were probably missed because they were positioned under actinarian tentacles. Larger rocks were another three-dimensional structure that was most common in Location 3 (Figure 17). *Ophiocomina nigra* was observed to aggregate on rocks, but sometimes it was not possible to see them properly because they were situated on the side of the rock and/or the three-dimensional structure would create a shadow that made it impossible to see the dark colored species. Another challenge related to three-dimensionality was posed by *O. nigra* itself. In areas where they were densely aggregated it could be impossible to distinguish individuals from each other and thus give a realistic estimate of the numbers of individuals. This is a challenge with visual methods that are not encountered with traditional grab sampling methods (Mackie, Coggan and van-Heteren, 2007).

#### 4.2.4 The effect of ambient light, water transparency and substrate

Comparable with shadows, *O. nigra* positioned on dark macroalgae was a challenge as they were well camouflaged on the dark patches of macroalgae. Using artificial light (lamps) could have been a solution to the challenge with shadows and *O. nigra* positioned on dark substrate. The ROV has a LED light under the camera in the front of the ROV. With the position chosen for the 360 camera, this was quite close to the light source (Figure 5 A). A LED light source can brighten up dark areas and give more natural colors to the objects. However, it will light up a limited area and the rest will be very dark (Ludvigsen, 2010). The light might also create new shadows due to the three-dimensionality of the seascape. As a result of the reasons mentioned, only natural light was used in this study. Natural light can be sufficient for imaging techniques in shallow waters, but surveys in deep water require artificial light due to the rapid attenuation of light in water (Sward, Monk and Barrett, 2019).

The ambient light in shallow waters is largely affected by the weather conditions (Preisendorfer, 1976). In May the sun created a larger contrast between light and dark areas in the shallowest areas of the transects. This led to larger areas with shadows where it for instance was not possible to see if *O. nigra* was present. In September there was a heavy rainfall that led to a large input of freshwater into Hopavågen. The freshwater carried organic matter and the surface waters in Hopavågen was colored brown due to an elevated concentration of cDOM, a phenomenon described to have happened in Hopavågen earlier (Teacă, Ungureanu and Mureşan, 2017). High concentrations of cDOM gives a yellow tint to images (Kjerstad, 2014), and this was evident in the images from Location 2 and 3 which were surveyed after the rainfall. This gave a better contrast between substrate and *O. nigra*, which made them easier to identify and count (Figure 13). The effect of substrate related to contrast was also apparent in Location 1 where the white shell sand contrasted with the dark *O. nigra* (Figure 11).

#### 4.3 Study design with ROV transects

Protocols for conducting surveys and standardization of methods are important to ensure quality of collected data and comparable results. Norway follows NS-EN 16260:2012, the Norwegian and European standard for visual seabed surveys, which gives directions for pilot surveys, mapping, and monitoring (Standard Norge, 2012). As previously discussed by Strømsholm (2018) this standard is not adapted to shallow water surveys. The standard states that transects in heterogenous habitats should be of 500m length, and that there should be more than 20m between still photographs for mapping surveys (Standard Norge, 2012). Both the length of transect and interval between images would not be suitable for this study. It is possible to switch to a longer tether or use a boat for conducting longer transects with the ROV, but this would be a survey of an entirely different spatial scale and resolution. By increasing the length of the transects and increase the frame grab interval according to the standard, a lot of information on biodiversity and habitat diversity would be lost. Mitchell and Coggan (2007) review different standards for remote video techniques (drop cameras, towed video sledges and ROVs), which also includes considerations related to the use of miniROVs. Reliable information on size of FOV and distance travelled are important factors mentioned for the accuracy of line transect (Mitchell and Coggan, 2007).

The ROV used did not have sensors for tracking the geolocation of the ROV. The intended solution was to choose a starting point on land, point out the desired direction for the transect, and use the heading information in the ROV Blueye app to keep a constant heading, aided by activation of the auto-heading option. However, the ROV is small and is affected by wind and current speed and direction. On several occasions the ROV was observed to drift with the current when it was at surface level, especially in Location 1 which was most exposed to currents. Some drift was also experienced underwater during transects, and the heading had to be adjusted to drive more against the direction of the current. The length of the tether used was 75 m, but this is not a reliable measurement of distance traveled, as the tether is also subjected to drag by currents (Ludvigsen, 2010). Consequently, the accuracy of geolocation and length of the transects from visit to visit was affected. The transect in Location 2, where the ROV was following the pipeline, was more repeatable than the other two transects. To have a physical reference on the seafloor greatly eased the geolocation of the ROV.

Due to a varying altitude (distance between seafloor and ROV) the images from the 360 camera each covered a different sized area on the seafloor. Consequently, the number of *O. nigra* might not be representative for the actual density present. One example is from Location 1 in May where 165, 33, and 109 *O. nigra* were counted in three consecutive images. When viewing these images, it is apparent that the 360 camera is much closer to the seafloor in the middle one, thus covering a smaller area than the two other images. To introduce a relative abundance scoring on a qualitative scale can be an efficient method to work around such challenges (Mitchell and Coggan, 2007), as demonstrated in this study with the qualitative density category for *O. nigra*. However, variability in altitude can influence the ability to identify organisms, as demonstrated by Kjerstad (2014). She found that 13 out of 14 taxa of benthic species were unidentifiable when the distance between OOI and the imaging sensor increased from 0.3 m to 1.1 m due to reduced spatial resolution and attenuation from IOPs. Consequently, an option to lock the ROV to a constant altitude and speed would have been more optimal for image quality (Johnsen *et al.*, 2013) and repeatability of the method (Mitchell and Coggan, 2007; Standard Norge, 2012).

## **4.4 Future perspectives**

### **4.4.1 Possibilities for the ROV with a 360 camera**

In the newest model of the Blueye ROV, Blueye X3, some of the challenges encountered in this study has been solved: the camera can be tilted and has a total vertical FOV of 115° which will give a better view of the seafloor. It also has options to add altimeter (ping sonar altimeter and echosounder) for “auto-altitude” control mode for a constant distance to the seafloor, and to add an acoustic positioning system (Blueye.no, 2022). New semi-autonomous options for constant speed and altitude and the possibility of underwater geolocation of the ROV is expected to make it easier to conduct this kind of survey, enable quantitative measurements, increase the repeatability when returning to the same survey area, and increase image quality and identification success of OOI (Johnsen *et al.*, 2016).



As the 360 camera was found to substantially increase the information gained from the surveys, it could be of value to develop an integrated solution of the 360 camera into the ROV system. Options that would enhance the use includes to get a live feed of the 360 video, be able to start and stop recording during dives, and to find a more hydrodynamic solution than the one used in this survey. The current setup with the 360 camera altered the stability of the ROV, and it would rock back and forth after an input on the controller. In addition, the underwater housing for the 360 camera was scratched after hitting rocks and the seafloor as it was protruding out far in front of the ROV. A damaged underwater housing will affect the quality of future video and images with that housing. One possible solution would be to use a different mount and attach it to the top of the ROV so that the 360 camera sticks out in front of the ROV above the ROV camera. This will however increase the distance between the 360 camera and OOI and will probably not be more hydrodynamic. Other solutions would have to be explored.

#### **4.4.2 *Ophiocomina nigra* as indicator**

Brittle star beds are a prominent feature on the seabed that is easy to detect and monitor with optical methods such as the one used in this study. Especially *O. nigra* is easy to identify in Norwegian waters where there are no similar looking species (Hansson, Cedhagen and Strand, 2013). The requirements of the species are relatively well known, thus monitoring of brittle star beds can pose as useful indicators for state and change within coastal environments (Hughes, 1998).

*Ophiocomina nigra* is a highly opportunistic species with a high flexibility in feeding methods (Fontaine, 1965; Moen and Svensen, 2020). The species has been observed to respond to organic enrichment and human activities in several cases: to macroalgae detritus from green algae blooms resulting from organic enrichment in Brittany, France (Blanchet-Aurigny *et al.*, 2012; Guillou, Blanchet-Aurigny and Le Goaster, 2013), aggregating on patches of remains of *Laminaria hyperborea* (Gunnerus) Foslie, 1884 after trawling in Hustadvika, Norway (G. Johnsen, personal communication, May 2022), aggregating close to sewage discharges in the Mediterranean coast (Allain, Romano and Semroud, 1978; Harmelin, Bouchon and Hong, 1981, as discussed by Guillou, Blanchet-Aurigny and Le Goaster, 2013), to increase in numbers over several years after adding fertilizers to an enclosed sea-loch (Raymont, 1950), and to aggregate close to coastal fish farms (Woodcock *et al.*, 2018; Keeley *et al.*, 2020). A population outbreak (Uthicke, Schaffelke and Byrne, 2009) of *O. nigra* in a previously unoccupied area would be detectable with the method used in this study and could indicate organic enrichment or loose macroalgae. It might be difficult to determine the cause of the population outbreak solely based on optical surveys because of the flexibility in feeding method exhibited by the species. However, if there is a known source of organic enrichment, the population outbreak indicates that the enrichment affects the ecosystem. The consequence can be homogenization of the benthic ecosystem if a generalist species as *O. nigra* outcompetes specialist species adapted to the original environment (Blanchet-Aurigny *et al.*, 2012).

#### 4.4.3 Machine learning and automatic identification (AI)

New and more efficient methods bring large amounts of data that needs to be managed, stored, and analyzed (Solan *et al.*, 2003). In this study the processing from video files to images and further analysis of the images was time-consuming. Especially the identification and counting of the number of brittle stars in each image was laborious. Automatic identification with machine learning is a possible solution to this. It took about 10 hours to write the code and to perform the training of the algorithm that was used for the automatic identification of *O. nigra*. After that the automatic identification was very fast (less than 1 second per image). In comparison it took roughly 2.5 minutes to count 100 *O. nigra* manually. With 54 out of 115 images from Location 1 containing more than 100 *O. nigra*, and a maximum number of 631 *O. nigra* counted in one image, this was a highly time-consuming job.

The algorithm was successful in not mistaking *Ophiura* sp. for *O. nigra* (Figure 19). However, there was potential for improvement in some situations. The algorithm showed a tendency to give false positives (Figure 19). The training data only included images with *O. nigra* present. The occurrence of false positives could have been reduced by including images of the seafloor without *O. nigra* (B. Kvæstad, personal communication, May 2022). The performance of the algorithm of 86.7% based on number *O. nigra* counted in every image can be considered sufficient for the accuracy level required for this study. Only an estimate that can indicate the density of *O. nigra* is needed and not the accurate number. The algorithm performed poorly in the edges of images (Figure 20 A) due to the chosen FOV, but this was because of a lack of identification in such areas by the marine biologist which resulted in lack of training of the algorithm for these situations. Another example of poor performance of the algorithm was on close-up images because there were few of this in the training set. The algorithm will evaluate its performance based on the given training data and will therefore not perform better than the data it is given (Pettit *et al.*, 2021). The training set used was rather small. Following from this the algorithm was only trained on a narrow set of situations. With machine learning it is possible, and needed, to keep assessing the performance of the algorithm and make continuous improvements as the data set increases. A biological expert will always be needed, but AI is a tool that can drastically reduce the workload that follow from advances in technology for efficient survey methods that generate large amounts of data (Solan *et al.*, 2003; Wang, Ma and Zhou, 2009). In addition, it has the potential to reduce the subjectivity and increase the accuracy of visual identification (Persello and Bruzzone, 2014). However, the potential bias now lies in the training data.

#### 4.4.4 Citizen science

The ROV used in this study is relatively cheap compared to large ROVs that additionally relies on specially trained people and an operational vessel to be used (Johnsen *et al.*, 2013; Mogstad, 2021). There are even cheaper miniROVs on the market, making them an accessible tool for enthusiasts for the marine environment. The increased availability and lowered threshold for use of miniROVs (Sward, Monk and Barrett, 2019) introduces a potential for citizen science projects, where members of the public and scientists collaborate to conduct scientific research. The use of citizen science projects has increased exponentially since the 1990s, supported by

the developments in technology. It is estimated to be as much as 500 ongoing citizen science projects in Europe related to the marine environment (Garcia-Soto *et al.*, 2021). Citizen science data has successfully been used to obtain information on species that are difficult to sample or follow, and to collect samples of and document rare species and phenomena (Johansen *et al.*, 2021; Ringvold *et al.*, 2021; Edelist *et al.*, 2022). Potential citizen science projects related to the method of this study could involve uploading of observations of e.g., marine litter, pollution, rare or invasive species, or indicators such as a population outbreak of *O. nigra*. Citizens can also be involved in annotation of ROV video for training of a machine learning algorithm, as in the ongoing project connected to the Koster Islands, Sweden (EU-Citizen.Science, 2022). Citizen science projects are mutually beneficial. The citizens get the opportunity to increase their knowledge of the marine environment and get an opportunity to participate in collecting data that can be used in decision making for the benefit of their local marine environment. Scientists can obtain large, long time data sets with substantially decreased effort required (Garcia-Soto *et al.*, 2021). With an increasing market for miniROVs directed towards public buyers, the contribution to subsea citizen science projects is no longer constricted to come from divers.

## 5 Conclusion

In this study the spatial distribution of brittle stars in shallow waters was assessed using a miniROV and a 360 camera. *Ophiocomina nigra* is a conspicuous species that was easily identified with this optical method. This species dominated the benthic habitat in one of the studied areas in all three seasons. In the other areas *O. nigra* was mainly found on elevated hard substrate and on patches of macroalgae. The variability between the different areas in the spatial distribution of this species can be related to food availability and reflect the flexibility in feeding strategies of the species. Brittle stars in the *Ophiura* genus were not possible to identify to species level. The spatial distribution of *Ophiura* sp. was correlated with fine sediments, which they were well camouflaged in. Their substrate preference is also hypothesized to be connected to their feeding strategy and access to benthic prey. Depth, season, and temperature was not determining factors for the distribution of brittle stars in this study.

The identification success of OOI with the 360 camera is dependent on several factors, including altitude, video resolution and choice of FOV in the editing software. These factors all affect the spatial resolution of the images. There is a trade-off between the spatial resolution and sensitivity of the sensor, and between spatial resolution and the size of FOV. The identification success is additionally affected by ambient light conditions, IOPs, substrate, the velocity of the ROV, the three-dimensionality of the seascape and geometric distortion in the images. Options for geopositioning and auto-altitude and -speed in newer ROV-models are expected to improve the performance of the ROV in such surveys and give the possibility of obtaining quantitative data.

The 360 camera substantially increased the information gained with minor additional expenses and time use. A subsequent challenge following from advances of efficient methods are to analyze and visualize large amounts of data. The MCA was a helpful tool for assessing possible correlations between the variables in the data set. Automatic identification of *O. nigra* with machine learning showed a promising accuracy of 86.7%. By increasing the size and variety of the training data set the algorithm can be further improved and machine learning can be a valuable tool for efficient image analysis. Machine learning can reduce the bias of manual image analysis. However, the performance is reliant on the quality and amount of training data.

The study additionally demonstrated a high variability in the seascape in a relatively small area compared to the vast ocean space. This demonstrates the importance of studying the seascape on a variety of spatiotemporal scales. The easy operation and increased availability of miniROVs introduces a potential for involvement of citizen science projects to aid scientists in efficient mapping and monitoring of benthic habitats.

## 6 References

- Allain, J. Y., Romano, J. C. and Semroud, R. (1978) *Ophiocomina nigra* (O.F. Muller) (Echinodermata, Ophiuroidea) dans la région d'Alger, *Pelagos*, 5, pp. 50-64.
- Alvsvåg, D. M. (2017) *Mapping of a seagrass habitat in Hopavågen, Sør-Trøndelag, with the use of an Autonomous Surface Vehicle combined with optical techniques*. Master's thesis, NTNU.
- Ambrose, W. (1993) Effects of predation and disturbance by ophiuroids on soft-bottom community structure in Oslofjord: results of a mesocosm study, *Marine ecology progress series. Oldendorf*, 97(3), pp. 225-236.
- Apple.com (2022) *Reorient 360 video in Final Cut Pro* [Digital image]. Available at: <https://support.apple.com/no-no/guide/final-cut-pro/ver4c4f3b4e4/mac> (Accessed: 14 February 2022).
- Aronson, R. B. and Harms, C. A. (1985) Ophiuroids in a Bahamian saltwater lake: The ecology of a Paleozoic-like community, *Ecology*, 66(5), pp. 1472-1483.
- Aronson, R. B. (1989) Brittlestar beds: low-predation anachronisms in the British Isles, *Ecology*, 70(4), pp. 856-865.
- Artsdatabanken (2022). Available at: <https://www.artsdatabanken.no/> (Accessed: 16 March 2022).
- Barbier, E. B. (2017) Marine ecosystem services, *Current Biology*, 27(11), pp. R507-R510. doi: 10.1016/j.cub.2017.03.020.
- Blanchet-Aurigny, A. *et al.* (2012) Multi-decadal changes in two co-occurring ophiuroid populations, *Marine Ecology Progress Series*, 460, pp. 79-90. doi: doi.org/10.3354/meps09784.
- Blanchet-Aurigny, A. *et al.* (2015) Trophic niche of two co-occurring ophiuroid species in impacted coastal systems, derived from fatty acid and stable isotope analyses, *Marine Ecology Progress Series*, 525, pp. 127-141. doi: 10.3354/meps11169.
- Blueye.no (2022). Available at: <https://www.blueye.no/> (Accessed: 8 May 2022).
- Boos, K. *et al.* (2010) Sediment preference and burrowing behaviour in the sympatric brittlestars *Ophiura albida* Forbes, 1839 and *Ophiura ophiura* (Linnaeus, 1758) (Ophiuroidea, Echinodermata), *Journal of Experimental Marine Biology and Ecology*, 393(1-2), pp. 176-181. doi: doi.org/10.1016/j.jembe.2010.07.021.
- Buhl-Mortensen, L., Hodnesdal, H. and Thorsnes, T. (2015) *The Norwegian sea floor - new knowledge from MAREANO for ecosystem-based management*. NGU.
- Canada Centre for Mapping and Earth Observation (2019) *Fundamentals of remote sensing*. Available at: <https://www.nrcan.gc.ca/maps-tools-and-publications/satellite-imagery-and-air-photos/tutorial-fundamentals-remote-sensing/9309> (Accessed: 29 September 2021).
- Capa, M. (2021) *Serpulidae Rafinesque, 1815*. Available at: <https://www.artsdatabanken.no/Pages/313953/Serpulidae> (Accessed: 13 May 2022).
- Davies, J. *et al.* (2001) *Marine monitoring handbook*. Peterborough: JNCC.
- De Ridder, C. and Lawrence, J. M. (1982) Food and feeding mechanisms: Echinoidea *Echinoderm nutrition*. CRC Press, pp. 57-115.
- De-Bastos, E. and Hill, J. (2016) *Ophiothrix fragilis* and/or *Ophiocomina nigra* brittlestar beds on sublittoral mixed sediment.
- DNV (2021) *Ocean's future to 2050*. Available at: <https://www.dnv.com/Publications/ocean-s-future-to-2050-report-213872> (Accessed: 14 May 2022).

- Edelist, D. *et al.* (2022) Tracking Jellyfish Swarm Origins Using a Combined Oceanographic-Genetic-Citizen Science Approach, *Frontiers in Marine Science*, pp. 486. doi: doi.org/10.3389/fmars.2022.869619.
- EU-Citizen.Science (2022) *Koster Seafloor Observatory*. Available at: <https://eu-citizen.science/project/334> (Accessed: 16 May 2022).
- European Environment Agency (2019) EUNIS habitat type hierarchical view. Available at: [https://eunis.eea.europa.eu/habitats-code-browser.jsp?expand=1#level\\_1](https://eunis.eea.europa.eu/habitats-code-browser.jsp?expand=1#level_1) (Accessed: 14 May 2022).
- Fontaine, A. R. (1965) The feeding mechanisms of the ophiuroid *Ophiocomina nigra*, *Journal of the Marine Biological Association of the United Kingdom*, 45(2), pp. 373-385. doi: doi.org/10.1017/S0025315400054904.
- Funk, C. J., Bryant, S. B. and Heckman Jr, P. J. (1972) *Handbook of underwater imaging system design*. Naval Undersea Center.
- Garcia-Soto, C. *et al.* (2021) Marine Citizen Science: Current state in Europe and new technological developments, *Frontiers in Marine Science*, 8. doi: doi.org/10.3389/fmars.2021.621472.
- Gietler, S. (2018) *Pixels and Camera Sensors*. Available at: <https://www.uwphotographyguide.com/underwater-photography-technical-information> (Accessed: 25 March 2022).
- GoPro (2021) *Debunking 5K and 4K camera resolutions + Why you want them*. Available at: <https://gopro.com/en/rs/news/using-gopro-as-5k-and-4k-action-camera> (Accessed: 25 March 2022).
- Guillou, M., Blanchet-Aurigny, A. and Le Goaster, E. (2013) Density fluctuations of the ophiuroids *Ophiothrix fragilis* and *Ophiocomina nigra* in the Bay of Douarnenez, Brittany, France, *Marine Biodiversity Records*, 6.
- Halpern, B. S. *et al.* (2008) A global map of human impact on marine ecosystems, *science*, 319(5865), pp. 948-952. doi: 10.1126/science.1149345.
- HandBrake Team (2022) HandBrake. Available at: <https://handbrake.fr/>.
- Hansson, H. G., Cedhagen, T. and Strand, M. (2013) *Nationalnyckeln till Sveriges flora och fauna. Tagghudingar-svalgsträngsdjur. Echinodermata-Hemichordata*. Uppsala: Artdatabanken, SLU.
- Harmelin, J. G., Bouchon, C. and Hong, J. S. (1981) Impact de la pollution sur la distribution des échinodermes des substrats durs en Provence (Méditerranée Nord-Occidentale), *Tethys*, 10, pp. 13-36.
- Hong, Y. *et al.* (2015) Deep dual-resolution networks for real-time and accurate semantic segmentation of road scenes, *Journal of Latex class files*, 14. doi: doi.org/10.48550/arXiv.2101.06085.
- Hughes, D. J. (1998) *Subtidal brittlestar beds. An overview of dynamics and sensitivity characteristics for conservation management of marine SACs*. (Scottish Association for Marine Science (UK Marine SACs Project)). Available at: [http://ukmpa.marinebiodiversity.org/uk\\_sacs/pdfs/britstar.pdf](http://ukmpa.marinebiodiversity.org/uk_sacs/pdfs/britstar.pdf).
- Husson, F. (2016) Multiple Correspondence Analysis (Part 4/4: Interpretation aids): YouTube. Available at: [https://www.youtube.com/watch?v=wTCuThGiy4w&ab\\_channel=Fran%C3%A7oisHusson](https://www.youtube.com/watch?v=wTCuThGiy4w&ab_channel=Fran%C3%A7oisHusson).
- Iken, K. *et al.* (2001) Food web structure of the benthic community at the Porcupine Abyssal Plain (NE Atlantic): a stable isotope analysis, *Progress in Oceanography*, 50(1-4), pp. 383-405. doi: 10.1016/S0079-6611(01)00062-3.
- Insta360.com (2022). Available at: <https://www.insta360.com/> (Accessed: 27 April 2022).

- Jangoux, M. (1982) Food and feeding mechanisms: Asteroidea *Echinoderm nutrition*. CRC Press, pp. 117-159.
- Johansen, E. *et al.* (2021) Assessing the value of a citizen science approach for ctenophore identification, *Frontiers in Marine Science*, pp. 1691. doi: doi.org/10.3389/fmars.2021.772851.
- Johnsen, G. *et al.* (2013) Underwater hyperspectral imagery to create biogeochemical maps of seafloor properties, in Watson, J. and Zielinski, O. (ed.) *Subsea optics and imaging*. Woodhead Publishing, pp. 508-540e.
- Johnsen, G. *et al.* (2016) The use of underwater hyperspectral imaging deployed on remotely operated vehicles - methods and applications, *IFAC-PapersOnLine*, 49(23), pp. 476-481. doi: doi.org/10.1016/j.ifacol.2016.10.451.
- Johnsen, G. *et al.* (2020) Operative Habitat Mapping and Monitoring in the Polar Night, in Berge, J., Johnsen, G. and Cohen, J. H. (ed.) *POLAR NIGHT Marine Ecology: Life and Light in the Dead of Night*. Springer, pp. 277-305.
- Kaiser, M. J. *et al.* (2011) *Marine Ecology: Processes, Systems, and Impacts*. 2. edn. Oxford University Press.
- Kassambara, A. (2017) *MCA - Multiple Correspondence Analysis in R: Essentials*. Available at: <http://www.sthda.com/english/articles/31-principal-component-methods-in-r-practical-guide/114-mca-multiple-correspondence-analysis-in-r-essentials/> (Accessed: 24 February 2022).
- Kassambara, A. and Mundt, F. (2020) factoextra: Extract and Visualize the Results of Multivariate Data Analyses. Available at: <https://CRAN.R-project.org/package=factoextra>.
- Keeley, N. *et al.* (2020) Mixed-habitat assimilation of organic waste in coastal environments—It's all about synergy!, *Science of the Total Environment*, 699, pp. 134281. doi: 10.1016/j.scitotenv.2019.134281.
- Kjerstad, I. (2014) *Underwater imaging and the effect of Inherent Optical Properties on image quality*. Master thesis, NTNU. Available at: <http://hdl.handle.net/11250/245550>.
- Lê, S., Josse, J. and Husson, F. (2008) FactoMineR: an R package for multivariate analysis, *Journal of statistical software*, 25, pp. 1-18. doi: 10.18637/jss.v025.i01.
- Ludvigsen, M. (2010) *An ROV toolbox for optical and acoustical seabed investigations*. Doctoral thesis, NTNU. Available at: <http://hdl.handle.net/11250/237885>.
- Mackie, A. S. Y., Coggan, R. and van-Heteren, S. (2007) Grab sampling, in Coggan, R., *et al.* (ed.) *Review of Standards and Protocols for Seabed Habitat Mapping*.
- Marion, P. v. (1996) Ecological studies in Hopavågen, a landlocked bay at Agdenes, Sør-Trøndelag, Norway, *Gunneria 71*, pp. 1-39.
- Mitchell, A. and Coggan, R. (2007) Remote video techniques, in Coggan, R., *et al.* (ed.) *Review of standards and protocols for seabed habitat mapping*. MESH, pp. 179-203.
- Moen, F. E. and Svensen, E. (2020) *Dyreliv i havet - norsk marin fauna*. 7th edn. Kolofon forlag.
- Mogstad, A. A. (2021) *Underwater hyperspectral imaging as a tool for benthic habitat mapping*. Doctoral thesis, NTNU. Available at: [https://folk.ntnu.no/assor/PhD%20Thesis/Aksel\\_Alstad\\_Mogstad\\_PhD.pdf](https://folk.ntnu.no/assor/PhD%20Thesis/Aksel_Alstad_Mogstad_PhD.pdf).
- Mortensen, T. (1924) *Pighude (Echinodermer)*. København: G.E.C Gads Forlag.
- Palumbi, S. R. and Hedgecock, D. (2005) The life of the sea: implications of marine population biology to conservation policy, in Norse, E. A. and Crowder, L. B. (ed.) *Marine conservation biology: the science of maintaining the sea's biodiversity*. Island Press, pp. 33-46.

- Park, J., Byun, S.-C. and Lee, B.-U. (2009) Lens distortion correction using ideal image coordinates, *IEEE Transactions on Consumer Electronics*, 55(3), pp. 987-991. doi: 10.1109/TCE.2009.5278053.
- Parry, D. M. *et al.* (2003) Identification of patch structure within marine benthic landscapes using a remotely operated vehicle, *Journal of Experimental Marine Biology and Ecology*, 285, pp. 497-511. doi: 10.1016/S0022-0981(02)00546-4.
- Persello, C. and Bruzzone, L. (2014) Active and semisupervised learning for the classification of remote sensing images, *IEEE Transactions on Geoscience and Remote Sensing*, 52(11), pp. 6937-6956. doi: 10.1109/TGRS.2014.2305805.
- Pettit, R. W. *et al.* (2021) Artificial intelligence, machine learning, and deep learning for clinical outcome prediction, *Emerging topics in life sciences*, 5(6), pp. 729-745. doi: 10.1042/ETLS20210246.
- Piepenburg, D. (2000) Arctic brittle stars (Echinodermata: Ophiuroidea), in Gibson, R. N. and Barnes, M. (ed.) *Oceanography and marine biology: an annual review*. USA and Canada: Taylor & Francis, pp. 189-256.
- Preisendorfer, R. W. (1976) *Hydrologic Optics. Volume 5. Properties*. Honolulu, Hawaii: US Dept. of Commerce, National Oceanic and Atmospheric Administration.
- Raymont, J. E. G. (1950) A Fish Cultivation Experiment in an Arm of a Sea-loch. IV. The Bottom Fauna of Kyle Scotnish, *Proceedings of the Royal Society of Edinburgh, Section B: Biological Sciences*, 64(1), pp. 65-108. doi: 10.1017/S0080455X00012030.
- Riisgård, H. and Banta, G. (1998) Irrigation and deposit feeding by the lugworm *Arenicola marina*, characteristics and secondary effects on the environment. A review of current knowledge, *Vie et Milieu/Life & Environment*, 48(4), pp. 243-257.
- Ringvold, H. *et al.* (2021) In situ recordings of large gelatinous spheres from NE Atlantic, and the first genetic confirmation of egg mass of *Illex coindetii* (Vérany, 1839)(Cephalopoda, Mollusca), *Scientific reports*, 11(1), pp. 1-22. doi: 10.1038/s41598-021-86164-8.
- Robbins, R. E. and Shick, J. M. (1980) Expansion-contraction behavior in the sea anemone *Metridium senile*: Environmental cues and energetic consequences *Nutrition in the Lower Metazoa*. Elsevier, pp. 101-116.
- RStudio Team (2022) RStudio: Integrated Development Environment for R. RStudio, PBC, Boston, MA. Available at: <http://www.rstudio.com/>.
- Sebens, K. P. and Koehl, M. A. R. (1984) Predation on zooplankton by the benthic anthozoans *Alcyonium siderium* (Alcyonacea) and *Metridium senile* (Actiniaria) in the New England subtidal, *Marine Biology*, 81(3), pp. 255-271. doi: 10.1007/BF00393220.
- Shumchenia, E. J. and King, J. W. (2010) Comparison of methods for integrating biological and physical data for marine habitat mapping and classification, *Continental Shelf Research*, 30(16), pp. 1717-1729. doi: 10.1016/j.csr.2010.07.007.
- Solan, M. *et al.* (2003) Towards a greater understanding of pattern, scale and process in marine benthic systems: a picture is worth a thousand worms, *Journal of Experimental Marine Biology and Ecology*, 285, pp. 313-338. doi: 10.1016/S0022-0981(02)00535-X.
- Southward, E. C. and Campbell, A. C. (2006) *Echinoderms: keys and notes for the identification of British species*. Shrewsbury: Field Studies Council.
- Stachowitsch, M. (1984) Mass mortality in the Gulf of Trieste: the course of community destruction, *Marine Ecology*, 5(3), pp. 243-264. doi: doi.org/10.1111/j.1439-0485.1984.tb00124.x.
- Standard Norge (2012) *Water quality - Visual seabed surveys using remotely operated and/or towed observation gear for collection of environmental data*. (NS-EN 16260:2012). Available at:



- <https://www.standard.no/no/nettbutikk/produktkatalogen/Produktpresentasjon/?ProductID=606849> (Accessed: 16 February 2021).
- Strømsholm, J. (2018) *Eyes beneath the surface - using a miniROV to reveal the habitat and dietary choices of the European shag*. Master's thesis, NTNU. Available at: <http://hdl.handle.net/11250/2504409>.
- Stöhr, S., O'Hara, T. D. and Thuy, B. (2012) Global diversity of brittle stars (Echinodermata: Ophiuroidea), *Plos one*, 7(3), pp. e31940. doi: 10.1371/journal.pone.0031940.
- Stöhr, S., O'Hara, T. D. and Thuy, B. (2022) World Ophiuroidea Database. Available at: <https://www.marinespecies.org/ophiuroidea> (Accessed: 15 March 2022).
- Sward, D., Monk, J. and Barrett, N. (2019) A systematic review of remotely operated vehicle surveys for visually assessing fish assemblages, *Frontiers in Marine Science*, 6, pp. 134. doi: 10.3389/fmars.2019.00134.
- Taylor, A. M. (1958) *Studies on the ecology of Manx Ophiuroidea*. Master's thesis, University of Liverpool.
- Teacă, A., Ungureanu, C. and Mureşan, M. (2017) Assessment of diversity and distribution of benthic communities in Hopavågen Bay, Sletvik area (Norway), *Geo-Eco-Marina*, (23), pp. 103-120.
- Uthicke, S., Schaffelke, B. and Byrne, M. (2009) A boom–bust phylum? Ecological and evolutionary consequences of density variations in echinoderms, *Ecological monographs*, 79(1), pp. 3-24. doi: doi.org/10.1890/07-2136.1.
- Vaissie, P., Monge, A. and Husson, F. (2021) Factoshiny: Perform Factorial Analysis from 'FactoMineR' with a Shiny Application. Available at: <https://CRAN.R-project.org/package=Factoshiny>.
- Vizzini, J. (2020) SnapMotion. Available at: <https://apps.apple.com/us/app/snapmotion-unlimited/id1024350410>.
- Wang, H., Ma, C. and Zhou, L. (2009) A brief review of machine learning and its application, *2009 international conference on information engineering and computer science, Wuhan, China*. IEEE, pp. 1-4.
- Warner, G. (1982) Food and feeding mechanisms: Ophiuroidea *Echinoderm nutrition*. CRC Press, pp. 161-181.
- Warner, G. F. (1971) On the ecology of a dense bed of the brittle-star *Ophiothrix fragilis*, *Journal of the Marine Biological Association of the United Kingdom*, 51(2), pp. 267-282.
- Wickham, H. *et al.* (2019) Welcome to the Tidyverse, *Journal of open source software*, 4(43), pp. 1686. doi: 10.21105/joss.01686.
- Woodcock, S. H. *et al.* (2018) Mobile epibenthic fauna consume organic waste from coastal fin-fish aquaculture, *Marine environmental research*, 137, pp. 16-23. doi: 10.1016/j.marenvres.2018.02.017.

